

Double-real radiation in hadronic top quark pair production as a proof of a certain concept

M. Czakon^a

^a *Institut für Theoretische Teilchenphysik und Kosmologie, RWTH Aachen University,
D-52056 Aachen, Germany*

Abstract

Using the recently introduced STRIPPER approach to double-real radiation, we evaluate the total cross sections for the main partonic channels of the next-to-next-to leading order contributions to top quark pair production in hadronic collisions: $gg \rightarrow t\bar{t}gg$, $gg \rightarrow t\bar{t}q\bar{q}$, $q\bar{q} \rightarrow t\bar{t}gg$, $q\bar{q} \rightarrow t\bar{t}q'q'$, $q' \neq q$. The results are given as Laurent expansions in ϵ , the parameter of dimensional regularization, at a number of m/E_{CM} values spreading the entire variation range, with m the mass of the top quark and E_{CM} the center-of-mass energy. We describe the details of our implementation and demonstrate its main properties: pointwise convergence and efficiency. We also prove the cancellation of leading divergences after inclusion of the double-virtual and real-virtual contributions. On a more technical note, we extended the double-soft current formulae to the case of massive partons.

1. Introduction

In [1] we have proposed STRIPPER (SecToR Improved Phase sPacE for real Radiation), a novel subtraction scheme for the evaluation of double-real radiation contributions in next-to-next-to leading order (NNLO) QCD calculations. As suggested by the name, it is the phase space that acquires a special rôle in our approach. Once it is suitably parameterized and decomposed, Laurent expansions of arbitrary infrared safe observables can be obtained without any analytic integration, by applying numerical Monte Carlo methods. An important feature of STRIPPER is its process independence. In the actual calculation, general subtraction terms are combined with process dependent amplitudes. The simplicity of our construction contrasted with the complexity of double-real radiation singularity structure may lead to scepticism. The present publication is meant to prove that STRIPPER delivers on its promises.

There are many other subtraction schemes for real radiation. At next-to-leading order (NLO), most calculations are done with the method of [2, 3], but other approaches are subject to active development [4, 5] (see also [6]). At the NNLO level, the situation is more complex. Much has been achieved with Sector Decomposition [7, 8, 9] and Antenna Subtraction [10, 11, 12, 13], but there are more specialised methods for colorless states [14] and, very recently, for massive final states [15]. General tools are also being developed in [16, 17, 18, 19, 20]. There were, of course, many other proposals [21, 22, 23], which have not been completely developed.

To demonstrate the virtues of STRIPPER, we have chosen hadronic top quark pair production, as it is of great phenomenological relevance, but its theoretical description is still incomplete. The current state of the art in the field is as follows

1. differential cross sections including complete off-shell effects and leptonic decays are known at NLO [24, 25] (until recently, they were only available in the narrow-width approximation [26, 27]);

*Preprint numbers: TTK-10-58, SFB/CPP-10-134

2. fixed order threshold expansions for the quark-annihilation and gluon-fusion channels are known at NNLO up to constants, both for the total cross section [28], and for the invariant mass distribution [29];
3. soft-gluon resummation for the previously mentioned channels is understood at the NNLL level for the total cross section [30, 31] (see also [32]), and selected differential distributions [33] (see also [34]);
4. mixed soft-gluon and Coulomb resummation is understood at the NNLL level as well [35];
5. two-loop virtual amplitudes are known analytically in the high-energy limit [36, 37], for the planar contributions [38, 39], and fermionic contributions in the quark-annihilation channel [40]; in the same channel, the full amplitude is known numerically [41];
6. one-loop squared amplitudes are known analytically at the NNLO level [42, 43];
7. one-loop real-virtual (one additional massless parton in the final state) amplitudes have been obtained in the course of several projects connected to top quark pair production in association with jets [44, 45, 46];
8. approximations of the one-loop real-virtual amplitudes are known in all singular limits involving only massless partons [47, 48, 49, 50, 51] (this is needed for the evaluation of the real-virtual contributions).

We are interested in an NNLO calculation. Schematically, the involved partonic cross sections are a sum of three terms mentioned already above

$$d\sigma_{t\bar{t}+X}^{\text{NNLO}} = d\sigma^{VV} + d\sigma^{RV} + d\sigma^{RR}, \quad (1)$$

where $d\sigma^{VV}$ denotes the double-virtual (two-loop and one-loop squared), $d\sigma^{RV}$ the real-virtual (one-loop with one additional parton), and $d\sigma^{RR}$ the double-real (tree-level with two additional partons) corrections. We will ignore the need for collinear renormalization, which involves lower order cross sections expanded to higher orders in ϵ , the parameter of dimensional regularization. These have been derived (although not published) for the analysis of [52].

Currently missing are the double-real and real-virtual contributions. Once these are known, one can provide complete NNLO cross sections beyond the known threshold expansions. The real-virtual contribution has a simpler singularity structure than the double-real, and should be obtainable once the soft-gluon current in the presence of heavy quarks has been derived.

As far as the double-real contribution is concerned, there are many partonic channels, which need to be considered in principle. Nevertheless, current phenomenological applications require the knowledge of the cross sections with gluon-gluon and quark-anti-quark initial states. This leads to our choice of the following channels

$$gg \rightarrow t\bar{t}gg, \quad gg \rightarrow t\bar{t}q\bar{q}, \quad q\bar{q} \rightarrow t\bar{t}gg, \quad q\bar{q} \rightarrow t\bar{t}q'\bar{q}'. \quad (2)$$

We will only consider the case $q' \neq q$, because the case of identical quarks is expected to be numerically irrelevant. In the present publication, we will provide numerical values for the cross sections for the four channels as function of m/E_{CM} .

The paper is organized as follows. In the next Section, we will discuss the phase space, its volume, parameterization and decomposition. Subsequently, we will describe the derivation of the subtraction terms, convergence and cancellation of leading divergences. In Section 4, we will describe the technical details of our implementation, demonstrate its efficiency and describe several tests. Section 5 contains the results of numerical simulations for the four chosen channels. Apart from the main text and Conclusions, the publication consists of a number of Appendices. They contain the collinear splitting functions, a discussion of the double-soft limit in the presence of massive partons, another approach to the collinear limit in the double-soft limit, the Born cross sections, and finally a list of the software that we have used.

2. Phase space

2.1. Volume

A numerical approach, as the one advocated here, poses substantial problems, when assessing the correctness of both the approach and implementation. We will, therefore, start by introducing the only truly non-trivial integral that relates to our computation, but can be evaluated entirely analytically: the volume of the phase space.

We are interested in the following class of processes

$$a(p_1) + b(p_2) \rightarrow t(q_1) + \bar{t}(q_2) + c(k_1) + d(k_2), \quad (3)$$

where a, b are initial and c, d final state partons, in particular $ab = gg$ or $q\bar{q}$, and $cd = gg$ or $q'\bar{q}'$. Additionally

$$p_1^2 = p_2^2 = k_1^2 = k_2^2 = 0, \quad q_1^2 = q_2^2 = m^2 \neq 0, \quad (4)$$

and as usual

$$s = (p_1 + p_2)^2. \quad (5)$$

Throughout this publication we will work in the partonic center-of-mass system.

The phase space measure in d -dimensions is

$$d\Phi_4 = \frac{d^{d-1}k_1}{(2\pi)^{d-1}2k_1^0} \frac{d^{d-1}k_2}{(2\pi)^{d-1}2k_2^0} \frac{d^{d-1}q_1}{(2\pi)^{d-1}2q_1^0} \frac{d^{d-1}q_2}{(2\pi)^{d-1}2q_2^0} (2\pi)^d \delta^{(d)}(k_1 + k_2 + q_1 + q_2 - p_1 - p_2), \quad (6)$$

with $d = 4 - 2\epsilon$ as usual. We wish to evaluate the integral of unity with this measure. The result will be given as a product of two functions

$$\int d\Phi_4 = P_4(s, \epsilon) \Phi(x, \epsilon), \quad (7)$$

with

$$x = \frac{1 - \beta}{1 + \beta}, \quad \beta = \sqrt{1 - \frac{4m^2}{s}}, \quad (8)$$

and P_4 the volume of the phase space in the purely massless case

$$P_4(s, \epsilon) = 2^{-11+6\epsilon} \pi^{-5+3\epsilon} \frac{\Gamma^4(1 - \epsilon)}{\Gamma(3 - 3\epsilon)\Gamma(4 - 4\epsilon)} s^{2-3\epsilon}, \quad (9)$$

which can be easily obtained from the imaginary part of the three-loop massless sunrise diagram [53]. By definition, the Φ function must satisfy two boundary conditions

$$\Phi(1, \epsilon) = 0, \quad \Phi(0, \epsilon) = 1. \quad (10)$$

The first of the above equations is just the vanishing of the phase space at threshold, which is located at $x = 1$. The second follows from the normalization in the massless case, which in turn corresponds to $x = 0$.

In order to obtain Φ , we will use the method of differential equations [54, 55]. To this end, we exploit again the fact that Φ is given, up to normalization, by the imaginary part of the three-loop sunrise diagram, this time with two massless and two massive lines, see Fig. 1. Reducing the mass derivatives of the three occurring master integrals using integration-by-parts identities, we obtain the following two equations

$$\frac{\partial}{\partial x} \left(\frac{(1+x)^4}{x^2} \Phi(x, \epsilon) \right) = \frac{(1+x)^3}{x^3} \left(2(x-1)\epsilon \Phi(x, \epsilon) + (1+x)^3 \frac{\partial \Psi(x, \epsilon)}{\partial x} \right), \quad (11)$$

$$\begin{aligned} \frac{\partial^2 \Psi(x, \epsilon)}{\partial x^2} - \frac{1 - 20x + 3x^2}{x(1-x^2)} \frac{\partial \Psi(x, \epsilon)}{\partial x} - \frac{24}{x(1+x)^2} \Psi(x, \epsilon) = \\ -\epsilon \left(\frac{1 - 22x + x^2}{x(1-x^2)} \frac{\partial \Psi(x, \epsilon)}{\partial x} + \frac{24(2-\epsilon)}{x(1+x)^2} \Psi(x, \epsilon) + \frac{2(1-2\epsilon)}{(1+x)^4} \Phi(x, \epsilon) \right), \end{aligned} \quad (12)$$

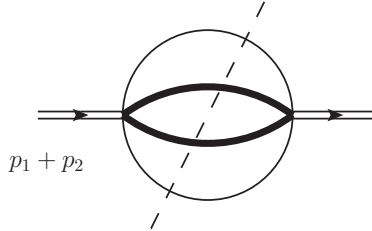


Figure 1: Three-loop sunrise graph used to obtain the phase space volume. Thick lines are massive, whereas the dashed line denotes a cut, which in this case corresponds to the imaginary part of the integral.

where we have only kept two of the master integrals, Φ and Ψ . Notice that Ψ 's sole purpose is to provide a solvable second order differential equation and a neat boundary condition, which follows again from the vanishing of the phase space at threshold

$$\Psi(1, \epsilon) = 0. \quad (13)$$

For this reason, we do not even bother specifying its exact definition.

With the three boundary conditions, the solution of the system of differential equations is unique, and can be obtained recursively as a series expansion in ϵ . In principle, we need five terms of the expansion corresponding to the five relevant terms of the expansion of the cross section, ranging from $1/\epsilon^4$ to ϵ^0 . As the expressions quickly become extremely lengthy, we will only reproduce the first two, and give a high precision numerical value at some benchmark point for the complete expansion¹. Φ is given by

$$\Phi(x, \epsilon) = \sum_{i=0}^{\infty} \epsilon^i \Phi^{(i)}(x), \quad (14)$$

¹The analytic result for $\Phi(x)$ is attached to the electronic preprint version of this publication

with

$$\Phi^{(0)}(x) = -\frac{48x^2 H(-1, 0, x)}{(x+1)^4} + \frac{24x^2 H(0, 0, x)}{(x+1)^4} + \frac{12(x^4 + 5x^3 + 6x^2 + 5x + 1) x H(0, x)}{(x+1)^6} - \frac{x^5 + 23x^4 + (34 + 4\pi^2)x^3 + (4\pi^2 - 34)x^2 - 23x - 1}{(x+1)^5}, \quad (15)$$

$$\begin{aligned} \Phi^{(1)}(x) = & -\frac{672x^2 H(-1, -1, 0, x)}{(x+1)^4} - \frac{96x^2 H(-1, 0, -1, x)}{(x+1)^4} + \frac{144x^2 H(-1, 0, 0, x)}{(x+1)^4} \\ & - \frac{480x^2 H(-1, 0, 1, x)}{(x+1)^4} + \frac{336x^2 H(0, -1, 0, x)}{(x+1)^4} + \frac{48x^2 H(0, 0, -1, x)}{(x+1)^4} \\ & - \frac{72x^2 H(0, 0, 0, x)}{(x+1)^4} + \frac{240x^2 H(0, 0, 1, x)}{(x+1)^4} - \frac{4(3x^2 + 56x + 3) x H(0, 0, x)}{(x+1)^4} \\ & + \frac{8(15x^4 + 122x^3 + 190x^2 + 122x + 15) x H(-1, 0, x)}{(x+1)^6} \\ & + \frac{24(x^4 + 5x^3 + 6x^2 + 5x + 1) x H(0, -1, x)}{(x+1)^6} \\ & + \frac{120(x^4 + 5x^3 + 6x^2 + 5x + 1) x H(0, 1, x)}{(x+1)^6} \\ & - \frac{4(2x^5 + 61x^4 + 4(50 + \pi^2)x^3 + 2(89 + 4\pi^2)x^2 + (86 + 4\pi^2)x + 13) x H(0, x)}{(x+1)^6} \\ & + \frac{(-2x^5 - 46x^4 + 4(8\pi^2 - 17)x^3 + 4(17 + 8\pi^2)x^2 + 46x + 2) H(-1, x)}{(x+1)^5} \\ & - \frac{10(x^5 + 23x^4 + 34x^3 - 34x^2 - 23x - 1) H(1, x)}{(x+1)^5} \\ & - \frac{2x(\pi^2(18x^4 + 43x^3 + 8x^2 + 43x + 18) + 180x(x+1)^2 \zeta_3)}{3(x+1)^6}. \end{aligned} \quad (16)$$

The H functions are standard harmonic polylogarithms (HPL) [56]. Their initial weight is 2, but the last term of the expansion we are interested in, *i.e.* ϵ^4 , contains HPLs up to weight six.

We can also obtain the behavior of Φ near threshold, either from the differential equations, or from the actual solution. The result is

$$\Phi\left(\frac{1-\beta}{1+\beta}, \epsilon\right) = \frac{64}{315} \beta^{9-10\epsilon} \left(1 + \mathcal{O}(\epsilon)\right) + \mathcal{O}(\beta^{10}). \quad (17)$$

The numerical benchmark expansion is chosen at $x = 1/2$

$$\begin{aligned} \Phi(1/2, \epsilon) = & 0.00001122829901964763 \\ & + 0.0001283543727784153 \epsilon \\ & + 0.0007325963156455679 \epsilon^2 \\ & + 0.002782712436211506 \epsilon^3 \\ & + 0.007910064621069109 \epsilon^4 \\ & + \mathcal{O}(\epsilon^5). \end{aligned} \quad (18)$$

One may wonder why it is not sufficient to test the implementation close to the massless case and avoid the work that led to the above expressions. The reason is that the presence of large logarithms of the mass, up to $\log^4(m^2/s)$, implies a high sensitivity of the result to the value of the small mass. A point like $x = 1/2$ has no special properties and, therefore, no large cancellations are expected.

Using the result for $\Phi(x)$ and its two derivatives in x , we have a complete set of master integrals and can evaluate the integral of any polynomial in scalar products of $p_1 + p_2$, $k_{1,2}$ and $q_{1,2}$. We will find it later useful to have the result for the following integral

$$\begin{aligned}
\int d\Phi_4 \left(\frac{k_1 \cdot q_1}{s} \right)^2 &= \frac{P_4(s, \epsilon)}{48(\epsilon - 1)^2 (12\epsilon^2 - 31\epsilon + 20) (1 - x)(1 + x)^4} \\
&\times \left((x + 1) (x^2 - 1) x^2 (\epsilon^2 (6x^2 - 8x + 6) + \epsilon (-19x^2 + 4x - 19) + 2 (7x^2 + 3x + 7)) \Phi''(x) \right. \\
&- (x + 1)x(2\epsilon^3 (5x^4 - 66x^3 + 82x^2 - 66x + 5) + \epsilon^2 (-47x^4 + 526x^3 - 210x^2 + 510x - 35) \\
&+ \epsilon (72x^4 - 636x^3 - 66x^2 - 628x + 34) + 4 (-9x^4 + 59x^3 + 26x^2 + 62x - 2)) \Phi'(x) \\
&- 2(x - 1)(2\epsilon^4 (x^4 + 60x^3 + 26x^2 + 60x + 1) - \epsilon^3 (11x^4 + 562x^3 + 470x^2 + 562x + 11) \\
&+ \epsilon^2 (22x^4 + 933x^3 + 1028x^2 + 933x + 22) - \epsilon (19x^4 + 660x^3 + 852x^2 + 660x + 19) \\
&\left. + 2 (3x^4 + 85x^3 + 122x^2 + 85x + 3)) \Phi(x) \right). \tag{19}
\end{aligned}$$

The value at our benchmark point is

$$\begin{aligned}
\frac{1}{P_4(s, \epsilon)} \int d\Phi_4 \left(\frac{k_1 \cdot q_1}{s} \right)^2 \Big|_{x=\frac{1}{2}} &= \tag{20} \\
&\left(1.4553533 + 16.673868 \epsilon + 95.377076 \epsilon^2 + 363.03219 \epsilon^3 + 1033.8027 \epsilon^4 + \mathcal{O}(\epsilon^5) \right) \times 10^{-9}.
\end{aligned}$$

2.2. Parameterization of the massless system

We will now introduce a suitable parameterization of the phase space. We will closely follow the lines of [1], where the massless system has been specified. In the next subsection, we will define a parameterization for the heavy system.

Before we give the momentum vectors, let us note that we can always choose them such that their ϵ -dimensional components vanish. This is due to the rotational invariance remaining in the system as long as we only have three vectors $\vec{p}_1, \vec{k}_1, \vec{k}_2$ (notice that $\vec{p}_2 = -\vec{p}_1$ by assumption). Therefore, we will specify the vectors, as if they were purely four-dimensional. The only consequence of the existence of the additional degrees of freedom is the modified form of the phase space measure, which is then sufficient to regulate all singularities. We will also exploit rotational invariance and space inversion invariance of the matrix elements (which can also be viewed as d -dimensional rotation invariance) to restrict the momenta as follows

$$k_1^x = 0, \quad k_2^x > 0. \tag{21}$$

In the actual Monte Carlo simulation, the momenta should be rotated randomly around the z -axis and the sign of x -axis should also be chosen at random, in order to fill out the complete phase space.

With the above assumptions, let

$$\begin{aligned}
p_1^\mu &= \frac{\sqrt{s}}{2} (1, 0, 0, 1), \\
p_2^\mu &= \frac{\sqrt{s}}{2} (1, 0, 0, -1), \\
n_1^\mu &= \frac{\sqrt{s}}{2} \beta^2 (1, 0, \sin \theta_1, \cos \theta_1), \\
n_2^\mu &= \frac{\sqrt{s}}{2} \beta^2 (1, \sin \phi \sin \theta_2, \cos \phi \sin \theta_2, \cos \theta_2), \\
k_1^\mu &= \hat{\xi}_1 n_1^\mu, \\
k_2^\mu &= \hat{\xi}_2 n_2^\mu, \tag{22}
\end{aligned}$$

where $\phi, \theta_{1,2} \in [0, \pi]$, and $n_{1,2}^\mu$ are auxiliary vectors needed to define soft limits, whereas $\hat{\xi}_{1,2}$ are used to parameterize the energies. Notice the hats above the variables. We shall use them to denote all variables, which are going to be transformed due to further phase space decomposition. The angular variables are replaced by another set in two steps.

We first define

$$\hat{\eta}_{1,2} = \frac{1}{2}(1 - \cos \theta_{1,2}), \quad (23)$$

$$\begin{aligned} \eta_3 &= \frac{1}{2}(1 - \cos \theta_3) \\ &= \frac{1}{2}(1 - \cos \phi \sin \theta_1 \sin \theta_2 - \cos \theta_1 \cos \theta_2) \\ &= \frac{1}{2}(1 - \cos(\theta_1 - \theta_2) + (1 - \cos \phi) \sin \theta_1 \sin \theta_2), \end{aligned} \quad (24)$$

where θ_3 is the relative angle between \vec{k}_1 and \vec{k}_2 , and by definition $\hat{\eta}_{1,2}, \eta_3 \in [0, 1]$. One of the main ideas of the subtraction scheme [1] is to change variables in such a way that all collinear limits be parameterized with just two variables, $\hat{\eta}_1$ and $\hat{\eta}_2$. In order to do so, we introduce

$$\zeta = \frac{1}{2} \frac{(1 - \cos(\theta_1 - \theta_2))(1 + \cos \phi)}{1 - \cos(\theta_1 - \theta_2) + (1 - \cos \phi) \sin \theta_1 \sin \theta_2} \in [0, 1], \quad (25)$$

which can be inverted to give

$$\eta_3 = \frac{(\hat{\eta}_1 - \hat{\eta}_2)^2}{\hat{\eta}_1 + \hat{\eta}_2 - 2\hat{\eta}_1\hat{\eta}_2 - 2(1 - 2\zeta)\sqrt{\hat{\eta}_1(1 - \hat{\eta}_1)\hat{\eta}_2(1 - \hat{\eta}_2)}}. \quad (26)$$

Clearly, the collinear limits are now at $\hat{\eta}_1 = 0, \hat{\eta}_2 = 0, \hat{\eta}_1 = 1, \hat{\eta}_2 = 1$ or $\hat{\eta}_1 = \hat{\eta}_2$. While $\theta_{1,2}$ are obtained from Eq. (23), ϕ is given by solving Eq. (24) and Eq. (26)

$$\cos \phi = \frac{1 - (1 - 2\hat{\eta}_1)(1 - 2\hat{\eta}_2) - \frac{2(\hat{\eta}_1 - \hat{\eta}_2)^2}{\hat{\eta}_1 + \hat{\eta}_2 - 2\hat{\eta}_1\hat{\eta}_2 - 2(1 - 2\zeta)\sqrt{\hat{\eta}_1(1 - \hat{\eta}_1)\hat{\eta}_2(1 - \hat{\eta}_2)}}}{4\sqrt{(1 - \hat{\eta}_1)\hat{\eta}_1(1 - \hat{\eta}_2)\hat{\eta}_2}}. \quad (27)$$

Notice that

$$\hat{\eta}_1 = \hat{\eta}_2 \Rightarrow \cos \phi = 1, \quad (28)$$

whereas

$$\hat{\eta}_1 = 0 \vee \hat{\eta}_2 = 0 \vee \hat{\eta}_1 = 1 \vee \hat{\eta}_2 = 1 \Rightarrow \cos \phi = 2\zeta - 1. \quad (29)$$

The last statement is valid, when $\hat{\eta}_1 \neq \hat{\eta}_2$, but seems to contradict implication (28). Fortunately, in the limiting cases $\hat{\eta}_1 = \hat{\eta}_2 = 0$ and $\hat{\eta}_1 = \hat{\eta}_2 = 1$ the momentum vectors do not depend on ϕ .

The final set of parameters specifying the kinematics of the massless partons is

$$\zeta, \hat{\eta}_1, \hat{\eta}_2, \hat{\xi}_1, \hat{\xi}_2. \quad (30)$$

The first three are unrestricted within the range $[0, 1]$, whereas the energy variables belong to one of the two non-overlapping regions (apart from a measure zero set) [1]

$$\{(\hat{\xi}_1, \hat{\xi}_2) : 0 \leq \hat{\xi}_1 \leq 1, 0 \leq \hat{\xi}_2 \leq \hat{\xi}_1 \xi_{max}(\hat{\xi}_1)\}, \quad (31)$$

$$\{(\hat{\xi}_1, \hat{\xi}_2) : 0 \leq \hat{\xi}_2 \leq 1, 0 \leq \hat{\xi}_1 \leq \hat{\xi}_2 \xi_{max}(\hat{\xi}_2)\}, \quad (32)$$

where

$$\xi_{max}(\xi) = \min\left(1, \frac{1}{\xi} \frac{1 - \xi}{1 - \beta^2 \eta_3 \xi}\right) \leq 1. \quad (33)$$

Not only do these conditions guarantee that the massive states can always be produced, but they are also suggestive of a decomposition of the phase space, which we will perform later on.

Having specified the parameterization of the phase space, we can rewrite the measure Eq. (6) in the new variables. We split it into two parts

$$d\Phi_4 = d\Phi_3(p_1 + p_2; k_1, k_2) d\Phi_2(Q; q_1, q_2) , \quad (34)$$

with

$$Q = p_1 + p_2 - k_1 - k_2 . \quad (35)$$

$d\Phi_3(p_1 + p_2; k_1, k_2)$ is not exactly the three-particle phase space of k_1, k_2 and Q , because the only constraint that it is subjected to is $Q^2 \geq 4m^2$. On the other hand, $d\Phi_2(Q; q_1, q_2)$ is the two-particle phase space. We have

$$\begin{aligned} d\Phi_3(p_1 + p_2; k_1, k_2) &= \frac{\pi^{2\epsilon}}{8(2\pi)^5 \Gamma(1-2\epsilon)} s^{2-2\epsilon} \beta^{8-8\epsilon} (\zeta(1-\zeta))^{-\frac{1}{2}-\epsilon} \\ &\times (\hat{\eta}_1(1-\hat{\eta}_1))^{-\epsilon} (\hat{\eta}_2(1-\hat{\eta}_2))^{-\epsilon} \frac{\eta_3^{1-2\epsilon}}{|\hat{\eta}_1 - \hat{\eta}_2|^{1-2\epsilon}} \hat{\xi}_1^{1-2\epsilon} \hat{\xi}_2^{1-2\epsilon} \\ &\times d\zeta d\hat{\eta}_1 d\hat{\eta}_2 d\hat{\xi}_1 d\hat{\xi}_2 . \end{aligned} \quad (36)$$

The first line above will be of no further concern, since we are only going to perform variable changes on the subset $\hat{\eta}_1, \hat{\eta}_2, \hat{\xi}_1, \hat{\xi}_2$. Therefore, we will define

$$d\mu_\zeta = \frac{\pi^{2\epsilon}}{8(2\pi)^5 \Gamma(1-2\epsilon)} s^{2-2\epsilon} \beta^{8-8\epsilon} (\zeta(1-\zeta))^{-\frac{1}{2}-\epsilon} d\zeta = \mu_\zeta d\zeta , \quad (37)$$

$$d\mu_{\eta\xi} = (\hat{\eta}_1(1-\hat{\eta}_1))^{-\epsilon} (\hat{\eta}_2(1-\hat{\eta}_2))^{-\epsilon} \frac{\eta_3^{1-2\epsilon}}{|\hat{\eta}_1 - \hat{\eta}_2|^{1-2\epsilon}} \hat{\xi}_1^{1-2\epsilon} \hat{\xi}_2^{1-2\epsilon} d\hat{\eta}_1 d\hat{\eta}_2 d\hat{\xi}_1 d\hat{\xi}_2 , \quad (38)$$

with $d\Phi_3 = d\mu_\zeta d\mu_{\eta\xi}$. Despite the splitting, $d\mu_{\eta\xi}$ depends on ζ through η_3 .

2.3. Parameterization of the massive system

In order to parameterize the massive system, we perform a boost to the center-of-mass frame of Q . Denoting the momenta of the heavy quarks in this frame by $q'_{1,2}$, we have

$$\begin{aligned} q_i^0 &= \frac{Q^0 q_i'^0 + \vec{Q} \cdot \vec{q}_i'}{\sqrt{Q^2}} , \\ \vec{q}_i' &= \vec{q}_i + \left(q_i'^0 + \frac{\vec{Q} \cdot \vec{q}_i'}{Q^0 + \sqrt{Q^2}} \right) \frac{\vec{Q}}{\sqrt{Q^2}} , \quad i = 1, 2 . \end{aligned} \quad (39)$$

The problem that we face is that once three $(d-1)$ -dimensional momenta of the massless partons have been specified with ϵ -dimensional components vanishing, we do not have the freedom to keep the latter components of $q'_{1,2}$ vanishing anymore. The easiest solution would be to restrict the momenta of the heavy quarks, which are always resolved after all, to lie in the four physical dimensions. This would simplify the parameterization, but we would lose the possibility to use the integrals derived in Section 2.1. Furthermore, to obtain finite partonic cross sections, it is necessary to add collinear counterterms, which are convolutions of splitting functions with lower order cross sections. If we would like to use the results obtained in [52] for this purpose, we need the heavy quarks in d -dimensions.

Let us, therefore, define the $q'_{1,2}$ momenta through three spherical angles θ_Q, ϕ_Q and ρ_Q .

$$\begin{aligned} q_1'^0 &= q_2'^0 = \frac{1}{2} \sqrt{Q^2} , \\ \vec{q}_1' &= -\vec{q}_2' = \frac{1}{2} \sqrt{Q^2 + \beta^2 - 1} \\ &\times (\sin \rho_Q \sin \phi_Q \sin \theta_Q \vec{n}^{(d-4)} , \cos \rho_Q \sin \phi_Q \sin \theta_Q , \cos \phi_Q \sin \theta_Q , \cos \theta_Q) . \end{aligned} \quad (40)$$

In principle, the three angles should lie in the range $[0, \pi]$. Nevertheless, we can assume $\phi_Q \in [0, 2\pi]$ and $\rho_Q \in [0, \pi/2]$, as long as we exploit the independence of the results from the sign of $\vec{n}^{(d-4)}$. In fact, without loss of generality, we can set

$$\vec{n}^{(d-4)} = (\vec{0}^{(d-5)}, 1), \quad (41)$$

and forget about the $(d-5)$ -dimensional components. Thus we have to work with five-dimensional vectors. We will soon see that the contribution of those vectors, which have a non-vanishing fifth dimension is suppressed by a power of ϵ as one would expect.

The two-particle phase space is now

$$\begin{aligned} d\Phi_2(Q; q_1, q_2) &= \frac{(4\pi)^\epsilon \Gamma(1-\epsilon)}{8(2\pi)^2 \Gamma(1-2\epsilon)} (Q^2)^{-\epsilon} \left(\sqrt{1 - \frac{4m^2}{Q^2}} \right)^{1-2\epsilon} (1 - \cos^2 \theta_Q)^{-\epsilon} (\sin^2 \phi_Q)^{-\epsilon} \\ &\times \frac{4^{1+\epsilon} \Gamma(-2\epsilon)}{\Gamma^2(-\epsilon) (1 - \cos^2 \rho_Q)^{1+\epsilon}} d \cos \theta_Q d \phi_Q d \cos \rho_Q \\ &= \mu_2 d \cos \theta_Q d \phi_Q d \cos \rho_Q. \end{aligned} \quad (42)$$

It depends on $\zeta, \hat{\eta}_{1,2}, \hat{\xi}_{1,2}$ only through Q^2 , although the momentum vectors $q_{1,2}$ depend on each of these variables independently. Close to threshold, where $Q^2 \approx s$, we recover the behavior Eq. (17)

$$\int d\Phi_4 \propto s^{2-3\epsilon} \beta^{9-10\epsilon}. \quad (43)$$

More interestingly, however, the ratio $\Gamma(-2\epsilon)/\Gamma^2(-\epsilon)$ is of the order ϵ , which means that we need a divergent contribution from the integral to obtain a cross section in four dimensions. This is indeed guaranteed by the following

$$\frac{4^{1+\epsilon} \Gamma(-2\epsilon)}{\Gamma^2(-\epsilon) (1 - \cos^2 \rho_Q)^{1+\epsilon}} = \delta(1 - \cos \rho_Q) + \frac{4^{1+\epsilon} \Gamma(-2\epsilon)}{\Gamma^2(-\epsilon)} \left[\frac{1}{(1 - \cos^2 \rho_Q)^{1+\epsilon}} \right]_+, \quad (44)$$

where the “+”-distribution is defined as

$$\int_0^1 d \cos \rho_Q \left[\frac{1}{(1 - \cos^2 \rho_Q)^{1+\epsilon}} \right]_+ f(\cos \rho_Q) = \int_0^1 d \cos \rho_Q \frac{1}{(1 - \cos^2 \rho_Q)^{1+\epsilon}} (f(\cos \rho_Q) - f(1)), \quad (45)$$

and the integrand on the right-hand side should be expanded in a Taylor series in ϵ . While we leave the discussion of the implementation details to Section 4, we note that we chose to use equation Eq. (44) to divide the phase space into two contributions

$$\begin{aligned} d\Phi_2 &= d\Phi_2^{(d|\epsilon)} + d\Phi_2^{(\epsilon)} \\ &= \mu_2^{(d|\epsilon)} d \cos \theta_Q d \phi_Q + \mu_2^{(\epsilon)} d \cos \theta_Q d \phi_Q d \cos \rho_Q, \end{aligned} \quad (46)$$

with

$$\begin{aligned} \mu_2^{(d|\epsilon)} &= \frac{(4\pi)^\epsilon \Gamma(1-\epsilon)}{8(2\pi)^2 \Gamma(1-2\epsilon)} (Q^2)^{-\epsilon} \left(\sqrt{1 - \frac{4m^2}{Q^2}} \right)^{1-2\epsilon} (1 - \cos^2 \theta_Q)^{-\epsilon} (\sin^2 \phi_Q)^{-\epsilon}, \quad (47) \\ \mu_2^{(\epsilon)} &= \frac{(16\pi)^\epsilon}{4(2\pi)^2 \Gamma(-\epsilon)} (Q^2)^{-\epsilon} \left(\sqrt{1 - \frac{4m^2}{Q^2}} \right)^{1-2\epsilon} (1 - \cos^2 \theta_Q)^{-\epsilon} (\sin^2 \phi_Q)^{-\epsilon} \\ &\times \left[\frac{1}{(1 - \cos^2 \rho_Q)^{1+\epsilon}} \right]_+. \end{aligned} \quad (48)$$

$d\Phi_2^{(d|\epsilon)}$ would be the entire phase space, if we could rotate the ϵ -dimensional components away. One can expect that the additional contribution from $d\Phi_2^{(\epsilon)}$ will be small in practice. We will show later that this is indeed the case.

At this point, we would like to note that the adopted solution to the problem of a d -dimensional phase space for the heavy quarks is by no means unique. One could, for example, use the fact that the ϵ -dimensional components of the heavy quark momentum vectors are only relevant to the terms singular in ϵ , which are obtained after one of the massless vectors has been removed (at least one soft or collinear limit). We then have only two $(d - 1)$ -dimensional vectors, and could rotate away the spurious components of $\vec{q}_{1,2}$. This approach would only be correct, if the reference frame for the parameterization of $\vec{q}_{1,2}$ were defined in relation to \vec{p}_1 and $\vec{k}_1 + \vec{k}_2$. This in turn, would be a simplification for the massive system, but a complication to the decomposition of the phase space, which we want to perform in Section 2.4.

2.4. Decomposition

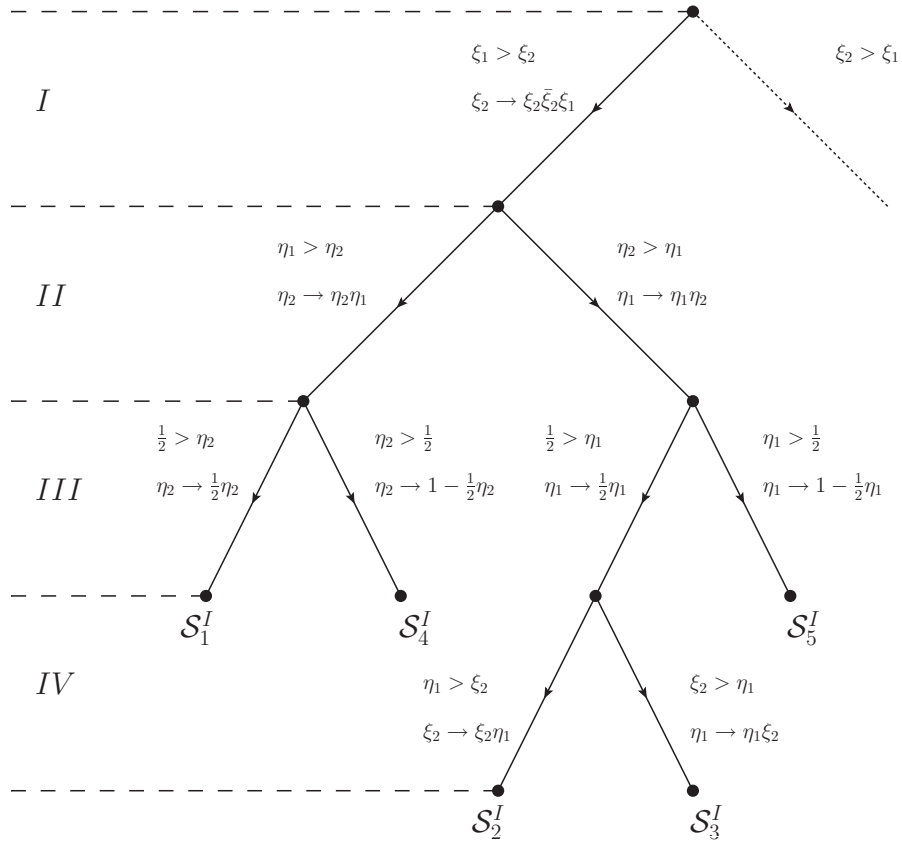


Figure 2: Decomposition of the phase space in the triple-collinear sector. The variable substitutions, which map the integration range onto the unit hypercube are specified. Furthermore, $\hat{\xi}_2 = \xi_{max}(\hat{\xi}_1)$ and the second branch starting with the dashed line is symmetric to the first.

The last step of our treatment of the phase space is a two-level decomposition according to singularities. At the first level, we partition the phase space with suitable selector functions. The latter are defined on the phase space, add up to unity, and regulate part of the divergences. In particular, we introduce a selector function for the triple-collinear sector, in which we allow for collinear divergences due to partons with momenta p_1 , k_1 and k_2 , but not p_2 . There is also a symmetric function that does just the same upon replacement of p_1 with p_2 , but we ignore it, as its contribution can be recovered without additional computation (see Section 4). Moreover, we introduce a selector, which allows for collinear divergences due to k_1 being parallel to p_1 , or k_2 parallel to p_2 , but no other configuration. This function defines the double-collinear sector, and

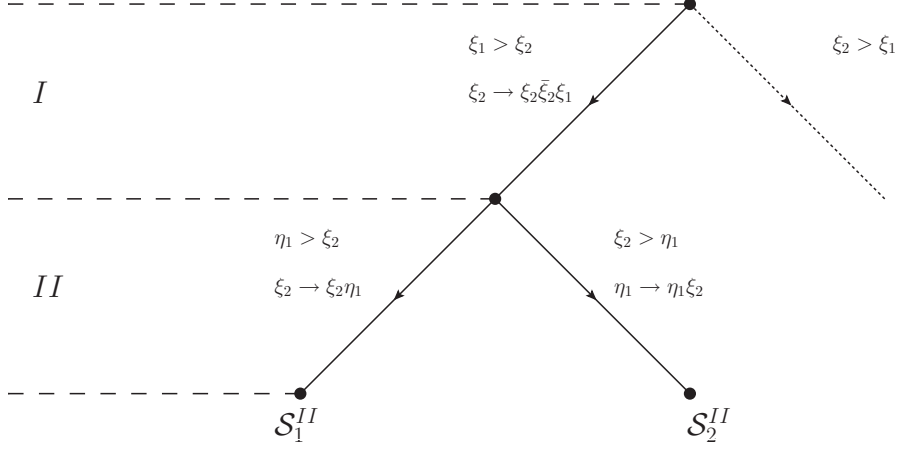


Figure 3: Decomposition of the phase space in the double-collinear sector. The notation is as in Fig. 2.

has a symmetric counterpart in $p_1 \leftrightarrow p_2$, which we again do not discuss any further. The triple- and double-collinear sectors may be overlapping in the sense that several selector functions do not vanish for a given momentum configuration. The only condition is that the divergences are properly regulated. In [1], we have given two examples of selector functions, which achieve this goal, one for our present problem, and one completely general for any number of massless final states. Apart from numerical efficiency, nothing depends on the choice. In the present work, we define the sectors implicitly as follows

1. $n_1^z > 0 \wedge n_2^z > -\alpha n_2^0$ in the triple-collinear sector;
2. $n_1^z > 0 \wedge n_2^z < -\alpha n_2^0$ in the double-collinear sector,

where $\alpha > 0$ is an arbitrary parameter, which we will take to be $\alpha = 1/2$ (we checked independence of some results on this parameter). Notice that the sharp cut $n_1^z > 0$ in both cases is necessary for the later use of symmetries. Moreover, we have defined the conditions through the vectors $n_{1,2}^\mu$, because in the strict soft limits the actual momentum vectors vanish and it is impossible to check to which sector they belong.

Having simplified the problem as far as the type of collinear singularities is concerned, we will perform a second level decomposition. The purpose is to factorize the divergences of the propagators in the amplitudes. The set of offending invariants is

$$\begin{aligned}
s_{15} &= (p_1 - k_1)^2 = -s\beta^2 \hat{\xi}_1 \hat{\eta}_1, \\
s_{16} &= (p_1 - k_2)^2 = -s\beta^2 \hat{\xi}_2 \hat{\eta}_2, \\
s_{26} &= (p_2 - k_2)^2 = -s\beta^2 \hat{\xi}_2 (1 - \hat{\eta}_2), \\
s_{56} &= (k_1 + k_2)^2 = s\beta^4 \hat{\xi}_1 \hat{\xi}_2 \eta_3, \\
s_{156} &= (p_1 - k_1 - k_2)^2 = -s\beta^2 (\hat{\xi}_1 \hat{\eta}_1 + \hat{\xi}_2 \hat{\eta}_2 - \beta^2 \hat{\xi}_1 \hat{\xi}_2 \eta_3), \\
s_{256} &= (p_2 - k_1 - k_2)^2 = -s\beta^2 (\hat{\xi}_1 (1 - \hat{\eta}_1) + \hat{\xi}_2 (1 - \hat{\eta}_2) - \beta^2 \hat{\xi}_1 \hat{\xi}_2 \eta_3). \tag{49}
\end{aligned}$$

Assuming that we are only concerned by the collinear singularities, $s_{15}, s_{16}, s_{56}, s_{156}$ are relevant to the triple-collinear sector, whereas s_{15}, s_{26} to the double-collinear sector. In case partons may also become soft, there will be soft-collinear singularities in the double-collinear sector due to s_{156} and s_{256} . Purely soft singularities may involve other propagators, in particular the massive, with a general form as follows

$$\begin{aligned}
(p + k_i)^2 - p^2 &= 2\hat{\xi}_i p \cdot n_i, \quad i = 1, 2, \\
(p + k_1 + k_2)^2 - p^2 &= 2(\hat{\xi}_1 p \cdot n_1 + \hat{\xi}_2 p \cdot n_2 + \hat{\xi}_1 \hat{\xi}_2 n_1 \cdot n_2). \tag{50}
\end{aligned}$$

Due to the polynomial form of the singular denominators, it is possible to factorize the divergences with a change of variables in such a way, that each expression be a product of variables to some powers, the variables themselves inducing divergences when vanishing, and a regular function. This is the well known sector decomposition [7]. The difference to the usual treatment is that, due to the process independent nature of singularities in QCD, we do not have to consider abstract expressions, but can view the decomposition as a choice of the order of the soft and collinear limits. A complete schematic representation of the variable transformations, which lead to factorization of divergences and specify the order of singular limits is given in Fig. 2 for the triple- and Fig. 3 for the double-collinear sector. Each level in these decomposition trees factorizes a certain type of singularities. For Fig. 2, we have

- I) factorization of the soft singularities;
- II, III) factorization of the collinear singularities;
- IV) factorization of the soft-collinear singularities.

The case of Fig. 3 is even simpler, as some of the levels disappear. Note that for each tree, we start with a new set of variables $\eta_{1,2} = \hat{\eta}_{1,2}$ and $\xi_{1,2} = \hat{\xi}_{1,2}$ at the root, and continue with the substitutions down to the leaves. The missing right branches corresponding to $\xi_2 > \xi_1$ can be recovered by changing the order of the final state partons. For this reason, we will ignore them as well. Finally, the variable substitutions guarantee that $\eta_{1,2}, \xi_{1,2} \in [0, 1]$, as the range Eq. (31) gets expanded.

Proving that this procedure is sufficient for factorization is a simple matter of substitutions and can be done with pen and paper. We shall not reproduce the uninteresting transformations here, since we shall not need them anymore. Nevertheless, we point out that the factorization of η_3 , present in s_{56} , introduces two regular functions, which we will encounter later. They are defined as

$$\begin{aligned} \eta_{31}(\eta_1, \eta_2) &= \frac{1}{\eta_1} \eta_3 \left(\eta_1, \frac{1}{2} \eta_1 \eta_2 \right) \\ &= \frac{(2 - \eta_2)^2}{2 \left(2 + \eta_2(1 - 2\eta_1) - 2(1 - 2\zeta) \sqrt{\eta_2(1 - \eta_1)(2 - \eta_1 \eta_2)} \right)}, \end{aligned} \quad (51)$$

$$\begin{aligned} \eta_{32}(\eta_1, \eta_2) &= \frac{1}{\eta_1 \eta_2^2} \eta_3 \left(\eta_1, \frac{1}{2} \eta_1 (2 - \eta_2) \right) \\ &= \frac{1}{2 \left(2 + (1 - 2\eta_1)(2 - \eta_2) - 2(1 - 2\zeta) \sqrt{(1 - \eta_1)(2 - \eta_2)(2 - \eta_1(2 - \eta_2))} \right)}, \end{aligned} \quad (52)$$

with $\eta_3(\hat{\eta}_1, \hat{\eta}_2)$ as in Eq. (26). The first of these functions is relevant to the sectors $\mathcal{S}_1^I, \dots, \mathcal{S}_3^I$, whereas the second to $\mathcal{S}_4^I, \mathcal{S}_5^I$. The derivation of the subtraction terms in Section 3.1 requires the knowledge of the behavior of $\eta_{31}(\eta_1, \eta_2)$ for small η_2

$$\eta_{31}(\eta_1, \eta_2) = 1 + (1 - 2\zeta) \sqrt{2(1 - \eta_1)\eta_2} + \mathcal{O}(\eta_2). \quad (53)$$

Tab. 1 contains the complete set of variable transformations, *i.e.* the expressions of the original kinematic variables $\hat{\eta}_{1,2}, \hat{\xi}_{1,2}$ in terms of the sector variables $\eta_{1,2}, \xi_{1,2}$. For the double-collinear sector, we have used the transformation $\eta_2 \rightarrow 1 - \eta_2$ first, in order to profit from the phase space measure Eq. (38), which is invariant under this transformation.

The above factorization procedure does not leave the phase space measure unchanged, even though it is only the factor $d\mu_{\eta\xi}$ that is transformed. The latter assumes, for a given sector \mathcal{S} , the following form

$$d\mu_{\eta\xi} = \eta_1^{a_1+b_1\epsilon} \eta_2^{a_2+b_2\epsilon} \xi_1^{a_3+b_3\epsilon} \xi_2^{a_4+b_4\epsilon} \mu_{\mathcal{S}}^{\text{reg}} d\eta_1 d\eta_2 d\xi_1 d\xi_2, \quad (54)$$

where the first factor regulates the divergences, whereas the second is a regular function, which we will later on expand in ϵ in a straightforward Taylor series. Both factors are given in Tab. 2.

	S_1^I	S_2^I	S_3^I	S_4^I	S_5^I	S_1^{II}	S_2^{II}
$\hat{\eta}_1$	η_1	$\frac{1}{2}\eta_1\eta_2$	$\frac{1}{2}\eta_1\eta_2\xi_2$	η_1	$\frac{1}{2}(2-\eta_1)\eta_2$	η_1	$\eta_1\xi_2$
$\hat{\eta}_2$	$\frac{1}{2}\eta_1\eta_2$	η_2	η_2	$\frac{1}{2}\eta_1(2-\eta_2)$	η_2	$1-\eta_2$	$1-\eta_2$
$\hat{\xi}_1$	ξ_1	ξ_1	ξ_1	ξ_1	ξ_1	ξ_1	ξ_1
$\hat{\xi}_2$	$\xi_1\xi_2\bar{\xi}_2$	$\eta_1\xi_1\xi_2\bar{\xi}_2$	$\xi_1\xi_2\bar{\xi}_2$	$\xi_1\xi_2\bar{\xi}_2$	$\xi_1\xi_2\bar{\xi}_2$	$\eta_1\xi_1\xi_2\bar{\xi}_2$	$\xi_1\xi_2\bar{\xi}_2$

Table 1: Original kinematic variables, $\hat{\eta}_1, \hat{\eta}_2, \hat{\xi}_1, \hat{\xi}_2$, expressed through the sector variables, $\eta_1, \eta_2, \xi_1, \xi_2$, with $\bar{\xi}_2 = \xi_{max}(\xi_1)$.

2.5. Normalization of the cross section

Although we have now specified the four-particle phase space completely, there is still a freedom in defining the divergent cross section for double-real radiation by including a function, which equals unity, when $\epsilon = 0$. Usually such a function is introduced due to the ϵ -dependence of the bare coupling constant, which, in the $\overline{\text{MS}}$ scheme, is chosen to be

$$\alpha_s^0 = \left(\frac{\mu^2 e^{\gamma_E}}{4\pi} \right)^\epsilon Z_{\alpha_s}(\alpha_s(\mu^2), \epsilon) \alpha_s(\mu^2), \quad (55)$$

where μ is the renormalization scale and Z_{α_s} the renormalization constant. Of course, in our case $Z_{\alpha_s} = 1$, since we are integrating tree-level amplitudes. The problem with this approach is that our matrix elements are proportional to α_s^4 , whereas the dimension of the phase space is the same as that of a three-loop integral. This would leave unbalanced, large and dimensionful factors of $\mu^{2\epsilon}$. We can compensate them by multiplying the cross section with the inverse of the parenthesized factor in Eq. (55) to power ϵ . Equivalently, we will express all tree level amplitudes by the renormalized strong coupling and use the following definition of the partonic cross section

$$\sigma_{\mathcal{O}} = \frac{1}{2s} \left(\frac{\mu^2 e^{\gamma_E}}{4\pi} \right)^{3\epsilon} \int d\Phi_4 F_J \overline{|\mathcal{M}_4|^2}, \quad (56)$$

where the overline over the matrix element squared signifies the sums and averages in color and spin, as well as statistical factors for identical final states. F_J is a jet function defining the observable \mathcal{O} . In what follows, we will mostly use a trivial jet function $F_J = 1$. Notice, however, that a test in Section 4 will be performed with a non-trivial F_J .

Let us stress, that we could have considered a different factor in Eq. (56), as long as we would include it in all the other contributions that enter the finite physical cross section. From the point of view of physics, this factor is irrelevant, and yet it can play a substantial rôle in obtaining precise numerical values. For example, multiplying by $\beta^{10\epsilon}$, we would remove dominant logarithms of β close to threshold, which would substantially lower the double-real cross section, while enhancing the others. We can also lower the contribution of the finite part of the cross section by multiplying with a constant, but ϵ dependent factor. The decision on what to enhance and what to diminish can only be taken once all terms are implemented in a numerical program, because only then can we check, what contributes the largest absolute errors. We will leave this problem to future studies.

sector	regulator	μ_S^{reg}
\mathcal{S}_1^I	$\eta_1^{1-2\epsilon} \eta_2^{-\epsilon} \xi_1^{3-4\epsilon} \xi_2^{1-2\epsilon}$	$((1-\eta_1)(2-\eta_1\eta_2))^{-\epsilon} \bar{\xi}_2^{2-2\epsilon} \left(\frac{\eta_{31}(\eta_1, \eta_2)}{2-\eta_2} \right)^{1-2\epsilon}$
\mathcal{S}_2^I	$\eta_1^{2-3\epsilon} \eta_2^{1-2\epsilon} \xi_1^{3-4\epsilon} \xi_2^{1-2\epsilon}$	$((1-\eta_2)(2-\eta_1\eta_2))^{-\epsilon} \bar{\xi}_2^{2-2\epsilon} \left(\frac{\eta_{31}(\eta_2, \eta_1)}{2-\eta_1} \right)^{1-2\epsilon}$
\mathcal{S}_3^I	$\eta_1^{-\epsilon} \eta_2^{1-2\epsilon} \xi_1^{3-4\epsilon} \xi_2^{2-3\epsilon}$	$((1-\eta_2)(2-\eta_1\eta_2\xi_2))^{-\epsilon} \bar{\xi}_2^{2-2\epsilon} \left(\frac{\eta_{31}(\eta_2, \eta_1\xi_2)}{2-\eta_1\xi_2} \right)^{1-2\epsilon}$
\mathcal{S}_4^I	$\eta_1^{1-2\epsilon} \eta_2^{1-2\epsilon} \xi_1^{3-4\epsilon} \xi_2^{1-2\epsilon}$	$((1-\eta_1)(2-\eta_2)(2-\eta_1(2-\eta_2)))^{-\epsilon} \bar{\xi}_2^{2-2\epsilon} \eta_{32}^{1-2\epsilon}(\eta_1, \eta_2)$
\mathcal{S}_5^I	$\eta_1^{1-2\epsilon} \eta_2^{1-2\epsilon} \xi_1^{3-4\epsilon} \xi_2^{1-2\epsilon}$	$((1-\eta_2)(2-\eta_1)(2-\eta_2(2-\eta_1)))^{-\epsilon} \bar{\xi}_2^{2-2\epsilon} \eta_{32}^{1-2\epsilon}(\eta_2, \eta_1)$
\mathcal{S}_1^{II}	$\eta_1^{2-3\epsilon} \eta_2^{-\epsilon} \xi_1^{3-4\epsilon} \xi_2^{1-2\epsilon}$	$((1-\eta_1)(1-\eta_2))^{-\epsilon} \bar{\xi}_2^{2-2\epsilon} \left(\frac{\eta_3}{ 1-\eta_1-\eta_2 } \right)^{1-2\epsilon}$
\mathcal{S}_2^{II}	$\eta_1^{-\epsilon} \eta_2^{-\epsilon} \xi_1^{3-4\epsilon} \xi_2^{2-3\epsilon}$	$((1-\eta_2)(1-\eta_1\xi_2))^{-\epsilon} \bar{\xi}_2^{2-2\epsilon} \left(\frac{\eta_3}{ 1-\eta_2-\eta_1\xi_2 } \right)^{1-2\epsilon}$

Table 2: Integration measure, $d\mu_{\eta\xi}$ expressed through the sector variables, $\eta_{1,2}, \xi_{1,2}$, decomposed into the product of their powers used to regulate the divergences, and a regular function, μ_S^{reg} , which can be expanded in ϵ .

3. Subtraction and integrated subtraction terms

3.1. Derivation

The decomposition of the phase space introduced in the previous sections is sufficient to derive Laurent expansions of arbitrary infrared safe observables. In order to obtain explicit expressions for a given sector \mathcal{S} , we define

$$\mathfrak{M}_{\mathcal{S}} = \eta_1^{1+a_1} \eta_2^{1+a_2} \xi_1^{1+a_3} \xi_2^{1+a_4} \overline{|\mathcal{M}_4|^2}, \quad (57)$$

where the a_i constants have been defined in Eq. (54), and are given for each sector in Tab. 2. The averaged matrix element, $\overline{|\mathcal{M}_4|^2}$, has been introduced in Eq. (56). $\mathfrak{M}_{\mathcal{S}}$ must be regular, by infrared power counting in QCD, in limits of any of $\eta_{1,2}, \xi_{1,2}$ vanishing. This can be checked explicitly, with the formulae introduced later in this section.

The cross section is now

$$\sigma_{\mathcal{O}} = \sum_{\mathcal{S}} \sigma_{\mathcal{O}}^{(\mathcal{S})}, \quad (58)$$

where

$$\begin{aligned}\sigma_{\mathcal{O}}^{(S)} &= \frac{1}{2s} \left(\frac{\mu^2 e^{\gamma_E}}{4\pi} \right)^{3\epsilon} \int d\mu_\zeta d\eta_1 d\eta_2 d\xi_1 d\xi_2 d\Phi_2 \mu_S^{\text{reg}} \theta_S F_J \frac{1}{\eta_1^{1-b_1\epsilon}} \frac{1}{\eta_2^{1-b_2\epsilon}} \frac{1}{\xi_1^{1-b_3\epsilon}} \frac{1}{\xi_2^{1-b_4\epsilon}} \mathfrak{M}_S \\ &= \int d\zeta d\eta_1 d\eta_2 d\xi_1 d\xi_2 d\cos\theta_Q d\phi_Q d\cos\rho_Q \Sigma_{\mathcal{O}}^{(S)},\end{aligned}\quad (59)$$

with the integrand

$$\Sigma_{\mathcal{O}}^{(S)} = \frac{1}{2s} \left(\frac{\mu^2 e^{\gamma_E}}{4\pi} \right)^{3\epsilon} \mu_\zeta \mu_S^{\text{reg}} \mu_2 \theta_S F_J \frac{1}{\eta_1^{1-b_1\epsilon}} \frac{1}{\eta_2^{1-b_2\epsilon}} \frac{1}{\xi_1^{1-b_3\epsilon}} \frac{1}{\xi_2^{1-b_4\epsilon}} \mathfrak{M}_S. \quad (60)$$

The b_i constants have been defined in Eq. (54), and are given for each sector in Tab. 2. The jet function F_J has been introduced in Eq. (56). Finally, θ_S is the selector function described at the beginning of Section 2.4. We remind the reader that the full phase space is covered by changing the order of the final state massless partons, and swapping p_1 and p_2 , which can also be thought of as changing the order of the initial state massless partons.

The Laurent expansion of the cross section contribution, $\sigma_{\mathcal{O}}^S$, is obtained by using

$$\frac{1}{\lambda^{1-b\epsilon}} = \frac{1}{b} \frac{\delta(\lambda)}{\epsilon} + \sum_{n=0}^{\infty} \frac{(b\epsilon)^n}{n!} \left[\frac{\ln^n(\lambda)}{\lambda} \right]_+, \quad (61)$$

where $\lambda = \eta_{1,2}, \xi_{1,2}$, and the “+”-distribution is

$$\int_0^1 d\lambda \left[\frac{\ln^n(\lambda)}{\lambda} \right]_+ f(\lambda) = \int_0^1 \frac{\ln^n(\lambda)}{\lambda} (f(\lambda) - f(0)). \quad (62)$$

A more practical, albeit equivalent, application of these formulae is

$$\int_0^1 \frac{d\lambda}{\lambda^{1-b\epsilon}} f(\lambda) \longrightarrow \int_0^1 d\lambda \left[\frac{f(0)}{b\epsilon} + \frac{f(\lambda) - f(0)}{\lambda^{1-b\epsilon}} \right]. \quad (63)$$

In any case, Eq. (59) involves four singular integrations and the above formula has to be applied iteratively. The result contains the integrand at sixteen different points obtained by setting the variables in all possible subsets of $\{\eta_1, \eta_2, \xi_1, \xi_2\}$ to zero. Using Eq. (63) gives a convergent integrand

$$\Sigma_{\mathcal{O}}^{(S)} \longrightarrow \left[\Sigma_{\mathcal{O}}^{(S)} \right]. \quad (64)$$

Considered differently, the terms in $\left[\Sigma_{\mathcal{O}}^{(S)} \right]$ proportional to negative powers of ϵ are called integrated subtraction terms, those free of singularities are simply called subtraction terms if any of the variables vanishes, just as in the classic approach to subtraction schemes. Notice that the only analytic integration that is needed here is the rather trivial integral of $1/\lambda^{1-b\epsilon}$. This is the main difference to the traditional approach. The limits of $d\Phi_2$, μ_S^{reg} , selector and jet functions are obtained by directly setting variables to zero, and are process independent. The only process dependent information is in \mathfrak{M}_S . The vanishing of the sector variables corresponds, however, to singular limits of QCD amplitudes. Thus, we can obtain the subtraction and integrated subtraction terms from the splitting functions and soft currents exactly as it is done at NLO. The sector decomposition of Section 2.4 guarantees the independence of the result from the order, in which the limits are taken. The process dependent information will now be shifted to reduced d -dimensional matrix elements.

In order to derive the relevant formulae, let $\mathbf{X} \subseteq \{\eta_1, \eta_2, \xi_1, \xi_2\}$ be the subset of vanishing variables in a given limit, and define

$$\lim_{\mathbf{X} \rightarrow 0} \mathfrak{M}_S = g^2 \langle \mathcal{M}_3 | \mathbf{V} | \mathcal{M}_3 \rangle \quad \text{or} \quad \lim_{\mathbf{X} \rightarrow 0} \mathfrak{M}_S = g^4 \langle \mathcal{M}_2 | \mathbf{V} | \mathcal{M}_2 \rangle, \quad (65)$$

depending on whether the Born matrix elements above correspond to reduced processes with one, $|\mathcal{M}_3\rangle$, or two partons, $|\mathcal{M}_2\rangle$, less. \mathbf{V} is an operator in spin and color space, and depends on the flavors of the partons involved. Let us also define a shorthand notation for the divergence regulating product of integration variables

$$\mathfrak{R}_S = \eta_1^{1+a_1} \eta_2^{1+a_2} \xi_1^{1+a_3} \xi_2^{1+a_4} . \quad (66)$$

We now consider the various limiting cases starting from those relevant to the triple-collinear sector. With the flavor assignment

$$a_1(p_1) + a_2(p_2) \rightarrow t(q_1) + \bar{t}(q_2) + a_5(k_1) + a_6(k_2) , \quad (67)$$

there are nine cases, which are identified from \mathbf{X} with the help of Tab. 1

1. $\boxed{\hat{\eta}_1 = \hat{\eta}_2 = 0}$

$$\mathbf{V}_{a_1 a_5 a_6}^{ss'} = \lim_{\mathbf{X} \rightarrow 0} \mathfrak{R}_S \frac{4\hat{P}_{a_1 a_5 a_6}^{ss'}}{s_{156}^2} . \quad (68)$$

The splitting functions $\hat{P}_{a_1 a_5 a_6}^{ss'}$ are given in Appendix A. They depend on the following variables

$$x_1 = -1 , \quad x_5 = \beta^2 \hat{\xi}_1 , \quad x_6 = \beta^2 \hat{\xi}_2 , \quad (69)$$

and

$$k_{\perp 1}^\mu = 0 , \quad k_{\perp 5}^\mu = \beta^2 \hat{\xi}_1 \sqrt{\hat{\eta}_1} \bar{k}_{\perp 5}^\mu , \quad k_{\perp 6}^\mu = \beta^2 \hat{\xi}_2 \sqrt{\hat{\eta}_2} \bar{k}_{\perp 6}^\mu(\hat{\eta}_1, \hat{\eta}_2) , \quad (70)$$

with

$$\begin{aligned} \bar{k}_{\perp 5}^\mu &= (0, 0, 1, 0) , \\ \bar{k}_{\perp 6}^\mu(\hat{\eta}_1, \hat{\eta}_2) &= \frac{1}{\hat{\eta}_1 + \hat{\eta}_2 - 2(1-2\zeta)\sqrt{\hat{\eta}_1 \hat{\eta}_2}} \\ &\times \left(0, 2|\hat{\eta}_1 - \hat{\eta}_2| \sqrt{\zeta(1-\zeta)}, 2\sqrt{\hat{\eta}_1 \hat{\eta}_2} - (\hat{\eta}_1 + \hat{\eta}_2)(1-2\zeta), 0 \right) . \end{aligned} \quad (72)$$

The last vector is symmetric and homogeneous in $\hat{\eta}_1$ and $\hat{\eta}_2$, $\bar{k}_{\perp 6}^\mu(\hat{\eta}_1, \hat{\eta}_2) = \bar{k}_{\perp 6}^\mu(\hat{\eta}_2, \hat{\eta}_1) = \bar{k}_{\perp 6}^\mu(1, \hat{\eta}_1/\hat{\eta}_2) = \bar{k}_{\perp 6}^\mu(1, \hat{\eta}_2/\hat{\eta}_1)$. Moreover

$$\bar{k}_{\perp 6}^\mu(1, \rho) = \bar{k}_{\perp 5}^\mu + \frac{1}{2} \sqrt{\frac{1-\zeta}{\zeta}} |1-\rho| \bar{k}_{\perp 0}^\mu + \mathcal{O}((1-\rho)^2) , \quad (73)$$

with

$$\bar{k}_{\perp 0}^\mu = (0, 1, 0, 0) . \quad (74)$$

This asymptotic behavior is necessary for \mathfrak{M}_S not to be singular. This limit is usually responsible for eight of the fifteen subtraction terms.

2. $\boxed{\hat{\eta}_1 = 0}$

$$\mathbf{V}_{a_1 a_5}^{ss'} = \lim_{\mathbf{X} \rightarrow 0} \mathfrak{R}_S \frac{2\hat{P}_{a_1 a_5}^{ss'}}{s_{15}} , \quad (75)$$

with

$$z = \frac{1}{1 - \beta^2 \hat{\xi}_1} , \quad k_{\perp}^\mu = (0, 0, 1, 0) . \quad (76)$$

3. $\boxed{\hat{\eta}_2 = 0}$

$$\mathbf{V}_{a_1 a_6}^{ss'} = \lim_{\mathbf{X} \rightarrow 0} \mathfrak{R}_S \frac{2\hat{P}_{a_1 a_6}^{ss'}}{s_{16}} , \quad (77)$$

with

$$z = \frac{1}{1 - \beta^2 \hat{\xi}_2} , \quad k_{\perp}^\mu = \left(0, 2\sqrt{\zeta(1-\zeta)}, 2\zeta - 1, 0 \right) . \quad (78)$$

4. $\hat{\eta}_1 = \hat{\eta}_2$

$$\mathbf{V}_{a_5 a_6}^{ss'} = \lim_{\mathbf{x} \rightarrow \mathbf{0}} \mathfrak{R}_S \frac{2\hat{P}_{a_5 a_6}^{ss'}}{s_{56}}, \quad (79)$$

with

$$z = \frac{\hat{\xi}_1}{\hat{\xi}_1 + \hat{\xi}_2}, \quad k_{\perp}^{\mu} = \left(0, \sqrt{1 - \zeta}, \text{sgn}(\hat{\eta}_2 - \hat{\eta}_1)(1 - 2\hat{\eta}_1)\sqrt{\zeta}, -2 \text{sgn}(\hat{\eta}_2 - \hat{\eta}_1)\sqrt{\hat{\eta}_1(1 - \hat{\eta}_1)\zeta} \right). \quad (80)$$

5. $\hat{\xi}_2 = 0 \wedge \hat{\eta}_2 \neq 0 \wedge \hat{\eta}_2 \neq 1 \wedge \hat{\eta}_2 \neq \hat{\eta}_1 \wedge a_6 = g$

$$\mathbf{V} = - \lim_{\mathbf{x} \rightarrow \mathbf{0}} \mathfrak{R}_S \frac{1}{\hat{\xi}_2^2} \sum_{ij=1}^5 \mathcal{S}_{ij}(n_2) \mathbf{T}_i \cdot \mathbf{T}_j, \quad (81)$$

where

$$\mathcal{S}_{ij}(k) = \frac{p_i \cdot p_j}{(p_i \cdot k)(p_j \cdot k)}, \quad (82)$$

and $p_{i,j}$ is one of p_1, p_2, q_1, q_2, k_1 . \mathbf{T}_i are the standard [2] color operators.

6. $\hat{\xi}_1 = \hat{\xi}_2 = 0 \wedge \hat{\eta}_{1,2} \neq 0 \wedge \hat{\eta}_{1,2} \neq 1 \wedge \hat{\eta}_1 \neq \hat{\eta}_2$

In the case of a gluon pair the limit is given by

$$\begin{aligned} \mathbf{V} &= \lim_{\mathbf{x} \rightarrow \mathbf{0}} \mathfrak{R}_S \quad (83) \\ &\times \left(\sum_{ijkl=1}^4 \frac{1}{2} \mathcal{S}_{ij}(\hat{\xi}_1 n_1) \mathcal{S}_{kl}(\hat{\xi}_2 n_2) \{ \mathbf{T}_i \cdot \mathbf{T}_j, \mathbf{T}_k \cdot \mathbf{T}_l \} - C_A \sum_{ij=1}^4 \mathcal{S}_{ij}(\hat{\xi}_1 n_1, \hat{\xi}_2 n_2) \mathbf{T}_i \cdot \mathbf{T}_j \right). \end{aligned}$$

This approximation is discussed in Appendix B, where we also define $\mathcal{S}_{ij}(k_1, k_2)$. In the case of a quark pair we have

$$\mathbf{V} = \lim_{\mathbf{x} \rightarrow \mathbf{0}} \mathfrak{R}_S T_F \sum_{ij=1}^4 \mathcal{I}_{ij}(\hat{\xi}_1 n_1, \hat{\xi}_2 n_2) \mathbf{T}_i \cdot \mathbf{T}_j, \quad (84)$$

with [57]

$$\mathcal{I}_{ij}(k_1, k_2) = \frac{(p_i \cdot k_1)(p_j \cdot k_2) + (p_j \cdot k_1)(p_i \cdot k_2) - (p_i \cdot p_j)(k_1 \cdot k_2)}{(k_1 \cdot k_2)^2 [p_i \cdot (k_1 + k_2)] [p_j \cdot (k_1 + k_2)]}, \quad (85)$$

and $p_{i,j}$ in the expressions above is one of p_1, p_2, q_1, q_2 .

7. $\hat{\eta}_1 = \hat{\xi}_2 = 0 \wedge \hat{\eta}_2 \neq 0 \wedge \hat{\eta}_2 \neq 1 \wedge a_6 = g$

$$\mathbf{V}_{a_1 a_5}^{ss'} = - \lim_{\mathbf{x} \rightarrow \mathbf{0}} \mathfrak{R}_S \frac{2\hat{P}_{a_1 a_5}^{ss'}}{s_{15}} \sum_{ij=1}^4 \frac{1}{\hat{\xi}_2^2} \mathcal{S}_{ij}(n_2) \mathbf{T}_i \cdot \mathbf{T}_j, \quad (86)$$

with the collinear parameters specified in Eq. (76), whereas $p_{i,j}$ in Eq. (82) is one of $p_1 - k_1, p_2, q_1, q_2$.

8. $\hat{\eta}_2 = \hat{\xi}_1 = 0 \wedge \hat{\eta}_1 \neq 0 \wedge \hat{\eta}_1 \neq 1 \wedge a_5 = g$

$$\mathbf{V}_{a_1 a_6}^{ss'} = - \lim_{\mathbf{x} \rightarrow \mathbf{0}} \mathfrak{R}_S \frac{2\hat{P}_{a_1 a_6}^{ss'}}{s_{16}} \sum_{ij=1}^4 \frac{1}{\hat{\xi}_1^2} \mathcal{S}_{ij}(n_1) \mathbf{T}_i \cdot \mathbf{T}_j, \quad (87)$$

with the collinear parameters specified in Eq. (78), whereas $p_{i,j}$ in Eq. (82) is one of $p_1 - k_2, p_2, q_1, q_2$.

$$9. \quad \boxed{\hat{\eta}_1 = \hat{\eta}_2 \wedge \hat{\xi}_1 = \hat{\xi}_2 = 0 \wedge \hat{\eta}_{1,2} \neq 0 \wedge \hat{\eta}_{1,2} \neq 1}$$

$$\mathbf{V}_{a_5 a_6} = \lim_{\mathbf{X} \rightarrow \mathbf{0}} \mathfrak{R}_S \mathbf{J}_\mu^\dagger (\hat{\xi}_1 n_1 + \hat{\xi}_2 n_2) \frac{2\hat{P}_{a_5 a_6}^{\mu\nu}}{s_{56}} \mathbf{J}_\nu (\hat{\xi}_1 n_1 + \hat{\xi}_2 n_2). \quad (88)$$

This approximation is discussed in Appendix C, and the collinear parameters are given in Eq. (80)

The conditions for the various limits have been chosen such that only one of the above expressions generates a non-vanishing \mathbf{V} for a given \mathbf{X} . We have also minimized the use of soft limits. For example, the double-soft limit contains the double-collinear and double-soft limit, nevertheless the expressions are much lengthier than the double-soft limit of the double-collinear limit, since the latter contains no color correlators. This is only a practical choice, since all expressions would give the same after taking into account color conservation.

The double-collinear sector requires the cases 2, 5, 6 and 7 from the triple-collinear sector, as well as the following

$$1. \quad \boxed{\hat{\eta}_1 = 0 \wedge \hat{\eta}_2 = 1}$$

$$\mathbf{V}_{a_1 a_5 a_2 a_6}^{s s' s'' s'''} = \lim_{\mathbf{X} \rightarrow \mathbf{0}} \mathfrak{R}_S \frac{2\hat{P}_{a_1 a_5}^{s s'}}{s_{15}} \frac{2\hat{P}_{a_2 a_6}^{s'' s'''}}{s_{26}}, \quad (89)$$

with the collinear variables defined in Eq. (76) for $\hat{P}_{a_1 a_5}^{s s'}$ and in Eq. (78) for $\hat{P}_{a_2 a_6}^{s'' s'''}$.

$$2. \quad \boxed{\hat{\eta}_2 = 1}$$

$$\mathbf{V}_{a_2 a_6}^{s s'} = \lim_{\mathbf{X} \rightarrow \mathbf{0}} \mathfrak{R}_S \frac{2\hat{P}_{a_2 a_6}^{s s'}}{s_{26}}, \quad (90)$$

with the collinear variables defined in Eq. (78).

$$3. \quad \boxed{\hat{\eta}_2 = 1 \wedge \hat{\xi}_1 = 0 \wedge \hat{\eta}_1 \neq 0 \wedge \hat{\eta}_1 \neq 1 \wedge a_5 = g}$$

$$\mathbf{V}_{a_2 a_6}^{s s'} = - \lim_{\mathbf{X} \rightarrow \mathbf{0}} \mathfrak{R}_S \frac{2\hat{P}_{a_2 a_6}^{s s'}}{s_{26}} \sum_{ij=1}^4 \frac{1}{\hat{\xi}_1^2} \mathcal{S}_{ij}(n_1) \mathbf{T}_i \cdot \mathbf{T}_j, \quad (91)$$

with the collinear parameters specified in Eq. (78), whereas $p_{i,j}$ in Eq. (82) is one of $p_1, p_2 - k_2, q_1, q_2$.

Since the \mathbf{V} operators are used both for subtraction and integrated subtraction terms, there is one more difference of the present approach to the traditional one. There will be transverse vectors k_\perp in the integrated subtraction terms. These are usually removed (averaged over) using the fact that once in the collinear limit, one can integrate over the azimuthal angle. Keeping them makes our approach less sensitive to simple errors, while not hampering efficiency.

We do not provide the explicit expressions for all the limits derived according to the rules above. On the one hand, it is easy to obtain them, on the other, the formulae are extremely lengthy. We believe that it only makes sense to provide a complete, general, working implementation of our subtraction scheme. We will return to this in the future.

There is one more aspect that we can discuss now, namely convergence. Due to the well known pointwise nature of the listed limits, when using polarized splitting kernels, the convergence of the cross section integrands will be pointwise. We can also assess the rate of convergence. Assume that one of the variables $x \in \{\eta_1, \eta_2, \xi_1, \xi_2\}$ is rescaled as $x \rightarrow \kappa x$, $\kappa \rightarrow 0$, while the others remain fixed. If $\kappa = 0$ implies $\hat{\xi}_1 = 0$ or $\hat{\xi}_2 = 0$ or $\hat{\eta}_1 = \hat{\eta}_2$, but neither $\hat{\eta}_{1,2} = 0$ nor $\hat{\eta}_{1,2} = 1$, then, ignoring logarithmic enhancements,

$$\left[\Sigma_{\mathcal{O}}^{(S)} \right] (\kappa x) \approx \left[\Sigma_{\mathcal{O}}^{(S)} \right] (x). \quad (92)$$

On the other hand, if $\kappa = 0$ implies any of $\hat{\eta}_1 = 0$, $\hat{\eta}_2 = 0$, $\hat{\eta}_1 = 1$, $\hat{\eta}_2 = 1$, then again up to logarithmic enhancements

$$\left[\Sigma_{\mathcal{O}}^{(S)}\right](\kappa x) \approx \frac{1}{\sqrt{\kappa}} \left[\Sigma_{\mathcal{O}}^{(S)}\right](x). \quad (93)$$

This is the well known inverse square root behavior of collinear limits. The lack of such a behavior in the case $\hat{\eta}_1 = \hat{\eta}_2$ is due to the dependence of the relative angle parameter η_3 on the difference $\hat{\eta}_1 - \hat{\eta}_2$, which is quadratic as seen in Eq. (26). Due to the iterative derivation of the integrand, rescaling several variables leads to a scaling, which can also be obtained iteratively from the above formulae. Let us stress, that unless the given limit is a single-soft limit for a final state quark, the unsubtracted integrand behaves as

$$\Sigma_{\mathcal{O}}^{(S)}(\kappa x) \approx \frac{1}{\kappa} \Sigma_{\mathcal{O}}^{(S)}(x). \quad (94)$$

3.2. Leading divergences and leading logs

We have stressed in the Introduction that one of the main ideas behind our subtraction scheme is to avoid any non-trivial analytic integration and perform the entire calculation purely numerically. It is, however, advantageous to have at least some analytic formulae to perform tests of the implementation. This was already our motivation in deriving the volume of the phase space. It turns out that we can also obtain the leading singularity in ϵ directly from the subtraction terms. After all, the $1/\epsilon^4$ term corresponds to $\eta_1 = \eta_2 = \xi_1 = \xi_2 = 0$, which means that the reduced matrix element is that of the leading order process. The integral in ζ is then trivial

$$\int_0^1 d\zeta \frac{1}{\sqrt{\zeta(1-\zeta)}} = \pi. \quad (95)$$

What remains is the two-particle phase space of the leading order cross section. In consequence, we obtain

$$\sigma_{gg \rightarrow t\bar{t}gg}^{RR} = 10C_A^2 \frac{1}{\epsilon^4} \left(\frac{\alpha_s}{4\pi}\right)^2 \sigma_{gg \rightarrow t\bar{t}}^B + \mathcal{O}\left(\frac{1}{\epsilon^3}\right), \quad (96)$$

$$\sigma_{q\bar{q} \rightarrow t\bar{t}gg}^{RR} = 2C_F(C_A + 4C_F) \frac{1}{\epsilon^4} \left(\frac{\alpha_s}{4\pi}\right)^2 \sigma_{q\bar{q} \rightarrow t\bar{t}}^B + \mathcal{O}\left(\frac{1}{\epsilon^3}\right), \quad (97)$$

$$\sigma_{gg \rightarrow t\bar{t}q\bar{q}}^{RR} = \mathcal{O}\left(\frac{1}{\epsilon^3}\right), \quad (98)$$

$$\sigma_{q\bar{q} \rightarrow t\bar{t}q'\bar{q}'}^{RR} = \mathcal{O}\left(\frac{1}{\epsilon^3}\right), \quad (99)$$

where σ^B is the Born cross section for the two channels and can be found in Appendix D. Later on, we will use these formulae to test the normalization and precision of our numerical calculation. At this point, we can, however, verify the cancellation of the $1/\epsilon^4$ singularities in the inclusive top quark pair production cross section, since the divergences of the other contributions can be found in the literature. Indeed, we have

$$\sigma_{gg \rightarrow t\bar{t}}^{VV} = (4C_A^2 + 4C_A^2) \frac{1}{\epsilon^4} \left(\frac{\alpha_s}{4\pi}\right)^2 \sigma_{gg \rightarrow t\bar{t}}^B + \mathcal{O}\left(\frac{1}{\epsilon^3}\right), \quad (100)$$

$$\sigma_{q\bar{q} \rightarrow t\bar{t}}^{VV} = (4C_F^2 + 4C_F^2) \frac{1}{\epsilon^4} \left(\frac{\alpha_s}{4\pi}\right)^2 \sigma_{q\bar{q} \rightarrow t\bar{t}}^B + \mathcal{O}\left(\frac{1}{\epsilon^3}\right). \quad (101)$$

The two color factors in the parentheses in both equations have a different origin. One is given by the two-loop virtual corrections and can be read off from the explicit results of [36, 37] in the high energy limit (under the assumption that the leading divergence is proportional to the exact Born matrix element). Otherwise, it can be obtained from the complete divergence structure presented

in [58]. The second color factor is given by the square of the one-loop matrix element, and is easily obtained with the help of the \mathbf{I} operator from [59].

We still need to derive the divergences of the real-virtual corrections. This is much more difficult, because the structure of the singular limits of one-loop amplitudes is not the same as that of tree-level amplitudes. In other words, it is not enough to just take the $1/\epsilon^2$ term from the one-loop amplitude using the \mathbf{I} operator and then use the same operator to obtain the $1/\epsilon^2$ divergences from the phase space integration. The situation seems to be even more involved, because this problem has never been studied for hadronic heavy quark production, where the initial states are also partons. Fortunately, the leading singularity is only due to the purely massless states and has to factorize, and since it is due to the soft and collinear limit, it is the same irrespective of whether we consider initial or final states. In view of these considerations, we can use the results obtained for jet cross sections in e^+e^- annihilation [18]. Applying the general formulae obtained there, we have

$$\sigma_{gg \rightarrow t\bar{t}g}^{RV} = -18C_A^2 \frac{1}{\epsilon^4} \left(\frac{\alpha_s}{4\pi}\right)^2 \sigma_{gg \rightarrow t\bar{t}}^B + \mathcal{O}\left(\frac{1}{\epsilon^3}\right), \quad (102)$$

$$\sigma_{q\bar{q} \rightarrow t\bar{t}g}^{RV} = -2C_F(C_A + 8C_F) \frac{1}{\epsilon^4} \left(\frac{\alpha_s}{4\pi}\right)^2 \sigma_{q\bar{q} \rightarrow t\bar{t}}^B + \mathcal{O}\left(\frac{1}{\epsilon^3}\right). \quad (103)$$

Combining the three contributions, we have indeed

$$\sigma_{gg \rightarrow t\bar{t}+X}^{\text{NNLO}} = \mathcal{O}\left(\frac{1}{\epsilon^3}\right), \quad (104)$$

$$\sigma_{q\bar{q} \rightarrow t\bar{t}+X}^{\text{NNLO}} = \mathcal{O}\left(\frac{1}{\epsilon^3}\right). \quad (105)$$

Proving the cancellation of all divergences is much more difficult, even though we know that the cross section is finite by the Kinoshita-Lee-Nauenberg and the factorization theorems (the latter to remove initial state collinear divergences). Let us only note, that it is possible to write the coefficients of the $1/\epsilon^3$ singularities through the Born cross sections using convolutions in the worst case. Nevertheless, we will refrain from this exercise.

The knowledge of the leading singularities can also be exploited in another way. Indeed, it allows to predict the leading logarithms of β . It is enough to know the d -dimensional behavior of the phase space near threshold, which we have derived in Eq. (17) as being $\beta^{-10\epsilon}$. Performing the expansion down to the finite part, we obtain

$$\sigma_{gg \rightarrow t\bar{t}gg}^{RR} = \frac{12500}{3} C_A^2 \log^4 \beta \left(\frac{\alpha_s}{4\pi}\right)^2 \sigma_{gg \rightarrow t\bar{t}}^B + \mathcal{O}(\log^3 \beta), \quad (106)$$

$$\sigma_{q\bar{q} \rightarrow t\bar{t}gg}^{RR} = \frac{2500}{3} C_F(C_A + 4C_F) \log^4 \beta \left(\frac{\alpha_s}{4\pi}\right)^2 \sigma_{q\bar{q} \rightarrow t\bar{t}}^B + \mathcal{O}(\log^3 \beta), \quad (107)$$

$$\sigma_{gg \rightarrow t\bar{t}q\bar{q}}^{RR} = \mathcal{O}(\log^3 \beta), \quad (108)$$

$$\sigma_{q\bar{q} \rightarrow t\bar{t}q'\bar{q}'}^{RR} = \mathcal{O}(\log^3 \beta). \quad (109)$$

Notice that the coefficients are very large. In fact they are about an order of magnitude larger than the coefficients of $\log^4 \beta$ in the total cross section [28]. This will be reflected in the very large values of the cross section near threshold.

4. Implementation

The implementation of the subtraction scheme described in the previous sections for the particular case of top quarks involves a large set of tree level matrix elements, which can, moreover, be spin and color correlated. There are many methods to evaluate these in four dimensions. Nevertheless, we decided to work in conventional dimensional regularization (CDR), thus keeping the full d -dimensional dependence of the matrix elements. A simple way to derive explicit expressions

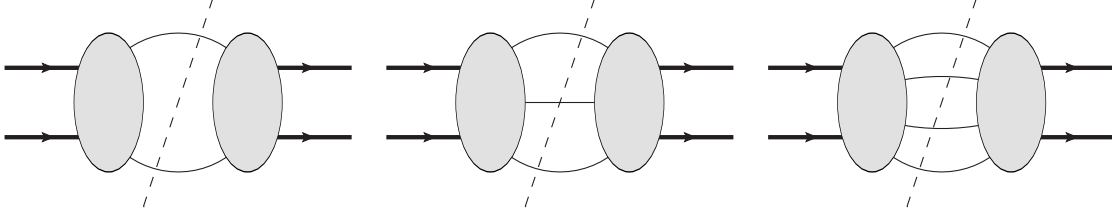


Figure 4: Cut graph classes used for generation of tree level amplitudes squared. The external thick lines represent top quarks, the cut thin lines are gluons, ghosts and light quarks, whereas blobs contain trees. Color operators may be assigned to each visible line on the left of the cut. Moreover, cut gluon lines may contain spin correlators.

in such a case is to generate cut graphs for forward scattering amplitudes with up to three loops. This procedure based on Cutkosky rules leaves the freedom of the choice of the external states, as any configuration can be obtained by crossing. We decided to take the top quarks on the external lines of the cut graphs. The tree-level amplitudes may have up to four external gluons, which means that there will be a lot of graphs related by symmetry (exchange of the gluon momenta). Taking the massless partons as virtual in the cut graphs takes care of the symmetry, in the sense that only one configuration is generated and one can symmetrize the complete amplitudes at the end. Thus, our expressions are substantially shorter than they would be, if we just squared tree-level amplitudes. Our procedure is a simpler version of the old approach of [60], but we would prefer the latter if we only had massless partons. The cut graph classes are shown in Fig. 4. We insert color operators \mathbf{T}_i to all external lines on the left of the cut, with up to four operators in total. We take the cut gluon propagators to be in the Feynman gauge and compensate the gauge invariance violation by cut ghost lines. We also insert spin correlators according to

$$\sum_{\lambda} \epsilon_{\lambda}^{\mu} \epsilon_{\lambda}^{\nu *} \longrightarrow \frac{1}{2} (k_{\perp 1}^{\mu} k_{\perp 2}^{\nu} + k_{\perp 1}^{\nu} k_{\perp 2}^{\mu}) , \quad (110)$$

where the symmetrized version is all that is required in practice, but one may need two different transverse vectors as demonstrated in Appendix A. As far as the color correlators are concerned, we have exploited color conservation to reduce the number of needed matrix elements. For an amplitudes with five partons, we have

$$\mathbf{T}_5 | \mathcal{M}_3 \rangle = -(\mathbf{T}_1 + \mathbf{T}_2 + \mathbf{T}_3 + \mathbf{T}_4) | \mathcal{M}_3 \rangle . \quad (111)$$

Moreover, since $\mathbf{T}_5^2 = C_A$ (for all the channels considered) or $\mathbf{T}_5^2 = C_F$ (in general), we have only five correlators to consider

$$\mathbf{T}_1 \cdot \mathbf{T}_2, \mathbf{T}_1 \cdot \mathbf{T}_3, \mathbf{T}_1 \cdot \mathbf{T}_4, \mathbf{T}_2 \cdot \mathbf{T}_3, \mathbf{T}_2 \cdot \mathbf{T}_4 . \quad (112)$$

Similarly, in the case of four-parton amplitudes, we have the following two double-correlators

$$\mathbf{T}_1 \cdot \mathbf{T}_2, \mathbf{T}_1 \cdot \mathbf{T}_3, \quad (113)$$

which may be additionally spin correlated. Amplitudes with four partons require, however, also quadruple-correlators. At the level of the amplitude

$$(\mathbf{T}_1 \cdot \mathbf{T}_2)(\mathbf{T}_1 \cdot \mathbf{T}_3) | \mathcal{M}_2 \rangle \neq (\mathbf{T}_1 \cdot \mathbf{T}_3)(\mathbf{T}_1 \cdot \mathbf{T}_2) | \mathcal{M}_2 \rangle , \quad (114)$$

nevertheless, since the matrix elements squared are real, we have

$$\begin{aligned} \langle \mathcal{M}_2 | (\mathbf{T}_1 \cdot \mathbf{T}_2)(\mathbf{T}_1 \cdot \mathbf{T}_3) | \mathcal{M}_2 \rangle &= \langle \mathcal{M}_2 | (\mathbf{T}_1 \cdot \mathbf{T}_2)(\mathbf{T}_1 \cdot \mathbf{T}_3) | \mathcal{M}_2 \rangle^* \\ &= \langle \mathcal{M}_2 | (\mathbf{T}_1 \cdot \mathbf{T}_3)^{\dagger} (\mathbf{T}_1 \cdot \mathbf{T}_2)^{\dagger} | \mathcal{M}_2 \rangle \\ &= \langle \mathcal{M}_2 | (\mathbf{T}_1 \cdot \mathbf{T}_3)(\mathbf{T}_1 \cdot \mathbf{T}_2) | \mathcal{M}_2 \rangle . \end{aligned} \quad (115)$$

amplitude	spin correlated lines	color correlated lines	amplitude	spin correlated lines	color correlated lines
$gg \rightarrow t\bar{t}gg$			$q\bar{q} \rightarrow t\bar{t}gg$		
$gg \rightarrow t\bar{t}q\bar{q}$			$q\bar{q} \rightarrow t\bar{t}q'\bar{q}'$		
$gg \rightarrow t\bar{t}g$			$q\bar{q} \rightarrow t\bar{t}q'q'$		
$gg \rightarrow t\bar{t}g$	1		$q\bar{q} \rightarrow t\bar{t}g$		
$gg \rightarrow t\bar{t}g$	2		$q\bar{q} \rightarrow t\bar{t}g$	5	
$gg \rightarrow t\bar{t}g$	5		$q\bar{q} \rightarrow t\bar{t}g$		(1,2)
$gg \rightarrow t\bar{t}g$		(1,2)	$q\bar{q} \rightarrow t\bar{t}g$		(1,3)
$gg \rightarrow t\bar{t}g$		(1,3)	$q\bar{q} \rightarrow t\bar{t}g$		(1,4)
$gg \rightarrow t\bar{t}g$		(1,4)	$q\bar{q} \rightarrow t\bar{t}g$		(2,3)
$gg \rightarrow t\bar{t}g$		(2,3)	$q\bar{q} \rightarrow t\bar{t}g$		(2,4)
$gg \rightarrow t\bar{t}g$		(2,4)	$q\bar{q} \rightarrow t\bar{t}$		
$gg \rightarrow t\bar{t}$			$q\bar{q} \rightarrow t\bar{t}$		(1,2)
$gg \rightarrow t\bar{t}$	1		$q\bar{q} \rightarrow t\bar{t}$		(1,3)
$gg \rightarrow t\bar{t}$	2		$q\bar{q} \rightarrow t\bar{t}$		(1,2)(1,2)
$gg \rightarrow t\bar{t}$	1,2		$q\bar{q} \rightarrow t\bar{t}$		(1,2)(1,3)
$gg \rightarrow t\bar{t}$		(1,2)	$q\bar{q} \rightarrow t\bar{t}$		(1,3)(1,3)
$gg \rightarrow t\bar{t}$		(1,3)			
$gg \rightarrow t\bar{t}$		(1,2)(1,2)	$\bar{q}q \rightarrow t\bar{t}$		
$gg \rightarrow t\bar{t}$		(1,2)(1,3)			
$gg \rightarrow t\bar{t}$		(1,3)(1,3)	$gq \rightarrow t\bar{t}q$		
$gg \rightarrow t\bar{t}$	1	(1,2)	$gq \rightarrow t\bar{t}q$		
$gg \rightarrow t\bar{t}$	1	(1,3)	$\bar{q}g \rightarrow t\bar{t}\bar{q}$		

Table 3: The 42 spin and color correlated amplitudes with four, five and six partons, which are needed for the four main channels of top quark pair production.

We thus only evaluate the following correlators

$$(\mathbf{T}_1 \cdot \mathbf{T}_2)(\mathbf{T}_1 \cdot \mathbf{T}_2), (\mathbf{T}_1 \cdot \mathbf{T}_2)(\mathbf{T}_1 \cdot \mathbf{T}_3), (\mathbf{T}_1 \cdot \mathbf{T}_3)(\mathbf{T}_1 \cdot \mathbf{T}_3). \quad (116)$$

Notice, that we have not exploited color conservation at the level of unsymmetrized amplitudes. This could provide another minor speedup.

Due to the selector functions and sectors chosen, we are missing phase space. Indeed, following Section 2.4, we have $k_1^z > 0$ and $k_1^0 > k_2^0$. For a given channel specified by flavor assignments to the initial and final partons, the additional contributions can be recovered by permuting initial and final states independently. Nevertheless, we can use charge conjugation invariance of QCD amplitudes together with rotation invariance, which allows to swap $p_1 \leftrightarrow p_2$, to reduce the number of configurations, which actually need to be evaluated. At the level of six-parton amplitudes, we only need the five cases

$$gg \rightarrow t\bar{t}gg, gg \rightarrow t\bar{t}q\bar{q}, q\bar{q} \rightarrow t\bar{t}gg, q\bar{q} \rightarrow t\bar{t}q'q', q\bar{q} \rightarrow t\bar{t}q'q'. \quad (117)$$

We will not explicitly mention the last amplitude anymore. Interestingly, however, its contribution is, for most cases, very close to that with swapped quark and anti-quark. The complete list of matrix elements is given in Tab. 3.

It is interesting to measure the evaluation time of the integrands for a single phase space point. The results of such a measurement are shown in Tab. 4. The main point of this table is to show that the subtraction and integrated subtraction terms are faster in evaluation than the matrix element of the double-real radiation process. This is true in all the cases, but the simplest involving six

process	matrix element [msec]	using HELAC [msec]	including subtraction [msec]	in quadruple precision [msec]
$gg \rightarrow t\bar{t}gg$	13	53	18	450
$q\bar{q} \rightarrow t\bar{t}gg$	0.71	6.5	0.81	27
$gg \rightarrow t\bar{t}q\bar{q}$	0.71	6.3	0.97	32
$q\bar{q} \rightarrow t\bar{t}q'\bar{q}'$	0.015	0.52	0.041	1.5

Table 4: Single phase space point timings for the evaluation of the matrix element with or without subtraction. The values in the fourth and fifth columns are the worst timings of all the seven sectors. The matrix elements of the present implementation have been compiled without optimization, because of the size of the expressions. Quadruple precision is obtained using the native implementation of the Intel Fortran compiler.

quarks. The latter has a very short expression for the amplitude, and it is simply impossible to have even simpler subtraction terms. One could, of course, suppose that the relative efficiency of the subtraction scheme is simply due to the very inefficient implementation of the six parton matrix elements themselves. That this is not the case is shown by comparing our implementation with that of HELAC [61, 62]. Reversing the argument, one could suppose that HELAC is inefficient, since our matrix elements have been obtained in the most naive way, and have, moreover, been compiled without optimization. This is not true in practice, as HELAC uses helicity sampling (or rather random polarization vectors), and has not been optimized for spin summed amplitudes, which we need here. It would certainly be advantageous to have an implementation of our scheme allowing for helicity sampling, as it was done in [63] at NLO. This requires, however, a tremendous effort, which we leave for the future. In Tab. 4, we have also quoted timings for computations in quadruple precision. In fact, we have used quadruple precision for all the values presented in the next section. Due to the cancellations inherent in subtraction schemes, there is always a risk of numerical instabilities. In this first study, we have not made any analysis in this direction, and decided to avoid the problem altogether using higher precision. This is certainly an issue, which requires improvements. We would also like to point out that the implementation of quadruple precision of the Intel Fortran compiler, which we used, is rather inefficient and we could have gained a speedup factor of at least two by switching to an external library.

Let us now discuss our implementation of the phase space integration. The evaluation of the cross sections requires seven- and eight-dimensional integrals, corresponding to the two contributions from the two-particle phase space Eq. (46). The integrands are indeed integrable, but not free of singularities. Besides logarithmic singularities due to the ϵ -expansion, there are inverse square root singularities as shown in Eq. (93). Our strategy is to use adaptive Monte Carlo integration techniques to improve convergence. We do not even bother with remappings for the square roots, which could perhaps help, but would be against our approach of avoiding any complications, unless, well, unavoidable. Thus, we use PARNI [64] to take care of all singularities. The seven sectors are evaluated with the same program in one run, and we even have implemented variance optimization *à la* stratified sampling, but we have not used this feature for the results presented here. The main computing time goes into the seven-dimensional integrals, as they involve the six-parton amplitudes. The eight-dimensional integrals have smaller contributions and are faster

per phase space point. They are thus negligible as far as resource requirements are concerned.

There is one more issue connected to numerics that we need to address, and that cannot be solved with higher precision. Inherent to subtraction is the fact that the integrands involve a cancellation of many digits close to singularities between the matrix elements and their approximations. If there were no inverse square roots, this might not have been a problem, but high precision of the results requires evaluation close to singularities. We thus need to cutoff the phase space to avoid instabilities. The form of the cutoff condition can be chosen at will, but since the matrix elements grow as $1/\eta_1\eta_2\xi_1\xi_2$, when the sector variables become small, we have decided to require the following

$$\eta_1 \eta_2 \xi_1 \xi_2 > \Delta . \quad (118)$$

The values we chose for Δ are given in the next section. Here, we evaluate the size the missing phase space due to this condition. In fact, one can show that

$$\delta\Phi_n(\Delta) = \int_0^1 \prod_{i=1}^n d\alpha_i \theta\left(\prod_{j=1}^n \alpha_j < \Delta\right) = \Delta \sum_{i=0}^{n-1} \frac{1}{i!} \log^i\left(\frac{1}{\Delta}\right) . \quad (119)$$

In our case $n = 4$. The size of the missing phase space cannot be used to estimate the implied error on the total cross section, due to the presence of square roots and logarithms. In practice, one evaluates the cross section at two values of the cutoff, say Δ and Δ' , with $\Delta' < \Delta$. It is expected that the improvement in the error will be of the order of $\sqrt{\Delta/\Delta'}$.

The final issue we would like to discuss is that of testing. In a project this size, it is important to check correctness at all stages. We have performed the following checks

1. Phase space volume We have evaluated the volume analytically in Section 2.1. By setting the matrix elements to unity, we can obtain a numeric result with our implementation. For example, with

$$s = 2 , \quad m = \frac{2}{3} , \quad \mu = \frac{1}{3} , \quad (120)$$

the exact value reads

$$\left(\frac{\mu^2 e^{\gamma_E}}{4\pi}\right)^{3\epsilon} \int d\Phi_4 = \left(5.9719120 + 87.151375 \epsilon + 630.84755 \epsilon^2 + 3019.2212 \epsilon^3 + 10746.200 \epsilon^4\right) \times 10^{-12} , \quad (121)$$

whereas 10 000 000 generated points suffice to obtain

$$\left(\frac{\mu^2 e^{\gamma_E}}{4\pi}\right)^{3\epsilon} \int d\Phi_4 \approx \left((5.9697 \pm 0.0028) + (87.131 \pm 0.033) \epsilon + (630.77 \pm 0.18) \epsilon^2 + (3019.2 \pm 0.64) \epsilon^3 + (10747 \pm 2.1) \epsilon^4\right) \times 10^{-12} . \quad (122)$$

2. ϵ -contribution to the two-particle phase space Section 2.1 contains a result for the integral of $(k_1 \cdot q_1)^2$. This integral is the simplest object sensitive to $d\Phi_2^{(\epsilon)}$. Unfortunately, the contribution is tiny at best. The analytic result for $s = 1, m^2 = \mu^2 = 2/9$ is

$$\frac{\mu^{6\epsilon}}{P_4(s, \epsilon)} \int d\Phi_4 \left(\frac{k_1 \cdot q_1}{s}\right)^2 = \left(1.4553533 + 10.106976 \epsilon + 34.956382 \epsilon^2 + 80.126733 \epsilon^3 + 136.49975 \epsilon^4\right) \times 10^{-9} , \quad (123)$$

whereas with very high statistics, we have

$$\begin{aligned} \frac{\mu^{6\epsilon}}{P_4(s, \epsilon)} \int d\Phi_4^{(d|\epsilon)} \left(\frac{k_1 \cdot q_1}{s} \right)^2 &= \left((1.45536 \pm 0.000014) + (10.1056 \pm 0.000085) \epsilon \right. \\ &\quad + (34.9482 \pm 0.00035) \epsilon^2 + (80.1058 \pm 0.0017) \epsilon^3 \\ &\quad \left. + (136.473 \pm 0.0084) \epsilon^4 \right) \times 10^{-9}, \end{aligned} \quad (124)$$

$$\begin{aligned} \frac{\mu^{6\epsilon}}{P_4(s, \epsilon)} \int d\Phi_4^{(\epsilon)} \left(\frac{k_1 \cdot q_1}{s} \right)^2 &= \left((0.001413 \pm 0.000011) \epsilon + (0.008145 \pm 0.000056) \epsilon^2 \right. \\ &\quad \left. + (0.02064 \pm 0.00013) \epsilon^3 + (0.02469 \pm 0.00020) \epsilon^4 \right) \times 10^{-9}. \end{aligned} \quad (125)$$

Clearly, there is disagreement between the $d\Phi_4^{(d|\epsilon)}$ values and Eq. (123) starting from order ϵ . Besides the highest order, ϵ^4 , the difference is at least at the level of 10σ . Together with the ϵ -contribution we obtain, however,

$$\begin{aligned} \frac{\mu^{6\epsilon}}{P_4(s, \epsilon)} \int d\Phi_4 \left(\frac{k_1 \cdot q_1}{s} \right)^2 &= \left((1.45536 \pm 0.000014) + (10.1070 \pm 0.000086) \epsilon \right. \\ &\quad + (34.9564 \pm 0.00035) \epsilon^2 + (80.1265 \pm 0.0017) \epsilon^3 \\ &\quad \left. + (136.498 \pm 0.0084) \epsilon^4 \right) \times 10^{-9}. \end{aligned} \quad (126)$$

3. Leading order cross sections With a jet function that forces all massless partons to be separated, we obtain the leading order cross section for top quark pair production in association with two jets. We use the following simple setup

$$k_{1,2} \cdot p_{1,2} > 10^{-4} s, \quad k_1 \cdot k_2 > 10^{-6} s, \quad (127)$$

together with

$$E_{\text{CM}} = 400 \text{ GeV}, \quad m_t = 172.6 \text{ GeV}, \quad \alpha_s(m_t) = 0.107639510785815. \quad (128)$$

We obtain

$$\sigma_{gg \rightarrow t\bar{t}gg} = (7.75 \pm 0.018) \times 10^{-2} \text{ nb}, \quad (129)$$

$$\sigma_{gg \rightarrow t\bar{t}q\bar{q}} = (4.81 \pm 0.019) \times 10^{-4} \text{ nb}, \quad (130)$$

$$\sigma_{q\bar{q} \rightarrow t\bar{t}gg} = (2.86 \pm 0.0065) \times 10^{-2} \text{ nb}, \quad (131)$$

$$\sigma_{q\bar{q} \rightarrow t\bar{t}q'\bar{q}'} = (3.55 \pm 0.010) \times 10^{-4} \text{ nb}, \quad (132)$$

whereas HELAC gives

$$\sigma_{gg \rightarrow t\bar{t}gg} = (7.76 \pm 0.039) \times 10^{-2} \text{ nb}, \quad (133)$$

$$\sigma_{gg \rightarrow t\bar{t}q\bar{q}} = (4.77 \pm 0.025) \times 10^{-4} \text{ nb}, \quad (134)$$

$$\sigma_{q\bar{q} \rightarrow t\bar{t}gg} = (2.88 \pm 0.0078) \times 10^{-2} \text{ nb}, \quad (135)$$

$$\sigma_{q\bar{q} \rightarrow t\bar{t}q'\bar{q}'} = (3.54 \pm 0.019) \times 10^{-4} \text{ nb}. \quad (136)$$

We point out that the results have been obtained with 1 000 000 Monte Carlo events, and our phase space parameterization seems to be more efficient than that of HELAC.

We have also checked our matrix elements for the six-parton processes at chosen phase space points against those obtained with HELAC. We have reached agreement within expected numerical accuracy.

4. Pointwise convergence in d -dimensions We can test the scaling given in Section 3.1 in all the limits, while expanding the results up to ϵ^4 . This has the advantage of showing that the subtraction terms are correct to all orders in ϵ , since the highest order of expansion of the matrix elements is ϵ^4 . The further terms of the expansion of $\left[\Sigma_{\mathcal{O}}^{(S)}\right]$ follow from the ϵ -dependence of the measure. We have evaluated all the fifteen limits of the seven sectors of the four main processes, which amounts to 420 cases. Needless to say, we obtained the correct behavior. To illustrate the tests, we only give one case, which sector \mathcal{S}_4^I of the process $gg \rightarrow t\bar{t}gg$ for the following configuration

$$s = 1, \beta = \frac{1}{2}, \zeta = \frac{1}{3}, \eta_1 = \frac{1}{4}, \eta_2 = \frac{1}{5} \times 10^{-40}, \xi_1 = \frac{1}{6}, \xi_2 = \frac{1}{7} \times 10^{-40},$$

$$\cos\theta_Q = \frac{1}{8}, \phi_Q = \frac{1}{9}, \cos\rho_Q = 1. \quad (137)$$

The results quoted correspond to $g_s = 1, \mu = m$, and we did not include the factors for spin and color averages, identical final states and flux. Without subtraction the integrand is

$$\begin{aligned} \Sigma^{(\mathcal{S}_4^I)} &= 2.92 \times 10^{79} + 1.14003 \times 10^{82} \epsilon + 2.22528 \times 10^{84} \epsilon^2 \\ &+ 2.89548 \times 10^{86} \epsilon^3 + 2.82539 \times 10^{88} \epsilon^4. \end{aligned} \quad (138)$$

The size of the coefficients is due to the expected growth of the integrand proportional to the inverse of the product of the four sector variables, which in this case is of the order 10^{80} . Once subtraction and integrated subtraction terms are included, the integrand becomes

$$\begin{aligned} \left[\Sigma^{(\mathcal{S}_4^I)}\right] &= 9.98769 \times 10^{-6} \frac{1}{\epsilon^4} + 0.0000869195 \frac{1}{\epsilon^3} + 0.00676374 \frac{1}{\epsilon^2} + 0.641465 \frac{1}{\epsilon} \\ &+ 40.9821 + 1961.23 \epsilon + 75083.4 \epsilon^2 + 2.39952 \times 10^6 \epsilon^3 + 6.61228 \times 10^7 \epsilon^4. \end{aligned} \quad (139)$$

We observe no growth of the coefficients, since the rescaling of η_2 and ξ_2 corresponds to the limit $\hat{\eta}_1 = \hat{\eta}_2$ and $\hat{\xi}_2 = 0$. Amongst all terms in $\left[\Sigma^{(\mathcal{S}_4^I)}\right]$, there is one that cancels the divergence of $\Sigma^{(\mathcal{S}_4^I)}$ alone, and contains the limit of $\mathfrak{M}_{\mathcal{S}}$ at $\hat{\eta}_1 = \hat{\eta}_2$ and $\hat{\xi}_2 = 0$. We can compare it order by order in ϵ to $\Sigma^{(\mathcal{S}_4^I)}$. The result is

$$\begin{aligned} \sum_{i=0}^4 \left(1 - \frac{\Sigma_{\text{approx}}^{(\mathcal{S}_4^I)}|_{\epsilon^i}}{\Sigma^{(\mathcal{S}_4^I)}|_{\epsilon^i}}\right) \epsilon^i &= -2.68 \times 10^{-41} - 2.68 \times 10^{-41} \epsilon - 2.68 \times 10^{-41} \epsilon^2 \\ &- 2.67 \times 10^{-41} \epsilon^3 - 2.67 \times 10^{-41} \epsilon^4. \end{aligned} \quad (140)$$

The very high numerical precision of these tests is important, because minor mistakes can sometimes show, for example, at the eight digit and would be impossible to find with a double precision implementation in Fortran. The above numbers have been obtained with an arbitrary precision implementation in MATHEMATICA. We have also compared quadruple precision results from Fortran with those of MATHEMATICA at ordinary points making sure that both implementations agree.

Further tests, most notably the agreement of the numerical values for the leading divergence with the analytic formulae from Section 3.2, as well as cutoff independence are described in the next section.

Finally, let us point out that this project has only been possible thanks to the use of complicated external software systems. These are listed in Appendix E.

β	ϵ^{-3}	ϵ^{-2}
0.001	$+3.501 \times 10^{-3} \pm 1.7 \times 10^{-6}$	$+1.245 \times 10^{-1} \pm 6.1 \times 10^{-5}$
0.025	$+4.796 \times 10^{-2} \pm 1.7 \times 10^{-5}$	$+9.312 \times 10^{-1} \pm 3.3 \times 10^{-4}$
0.075	$+1.026 \times 10^{-1} \pm 3.9 \times 10^{-5}$	$+1.422 \times 10^0 \pm 5.2 \times 10^{-4}$
0.125	$+1.377 \times 10^{-1} \pm 5.7 \times 10^{-5}$	$+1.544 \times 10^0 \pm 6.0 \times 10^{-4}$
0.175	$+1.603 \times 10^{-1} \pm 6.8 \times 10^{-5}$	$+1.512 \times 10^0 \pm 6.2 \times 10^{-4}$
0.225	$+1.731 \times 10^{-1} \pm 7.5 \times 10^{-5}$	$+1.393 \times 10^0 \pm 6.1 \times 10^{-4}$
0.275	$+1.777 \times 10^{-1} \pm 8.0 \times 10^{-5}$	$+1.225 \times 10^0 \pm 5.6 \times 10^{-4}$
0.325	$+1.750 \times 10^{-1} \pm 8.2 \times 10^{-5}$	$+1.025 \times 10^0 \pm 5.1 \times 10^{-4}$
0.375	$+1.662 \times 10^{-1} \pm 8.0 \times 10^{-5}$	$+8.134 \times 10^{-1} \pm 4.5 \times 10^{-4}$
0.425	$+1.520 \times 10^{-1} \pm 7.6 \times 10^{-5}$	$+6.006 \times 10^{-1} \pm 3.9 \times 10^{-4}$
0.475	$+1.332 \times 10^{-1} \pm 7.9 \times 10^{-5}$	$+3.978 \times 10^{-1} \pm 3.9 \times 10^{-4}$
0.525	$+1.108 \times 10^{-1} \pm 6.4 \times 10^{-5}$	$+2.132 \times 10^{-1} \pm 6.5 \times 10^{-4}$
0.575	$+8.609 \times 10^{-2} \pm 5.6 \times 10^{-5}$	$+5.670 \times 10^{-2} \pm 2.9 \times 10^{-4}$
0.625	$+5.967 \times 10^{-2} \pm 4.8 \times 10^{-5}$	$-6.833 \times 10^{-2} \pm 2.7 \times 10^{-4}$
0.675	$+3.315 \times 10^{-2} \pm 4.1 \times 10^{-5}$	$-1.548 \times 10^{-1} \pm 3.2 \times 10^{-4}$
0.725	$+7.890 \times 10^{-3} \pm 3.6 \times 10^{-5}$	$-1.983 \times 10^{-1} \pm 2.5 \times 10^{-4}$
0.775	$-1.472 \times 10^{-2} \pm 4.0 \times 10^{-5}$	$-1.974 \times 10^{-1} \pm 2.2 \times 10^{-4}$
0.825	$-3.278 \times 10^{-2} \pm 3.9 \times 10^{-5}$	$-1.540 \times 10^{-1} \pm 1.8 \times 10^{-4}$
0.875	$-4.402 \times 10^{-2} \pm 4.0 \times 10^{-5}$	$-7.173 \times 10^{-2} \pm 1.5 \times 10^{-4}$
0.925	$-4.497 \times 10^{-2} \pm 3.2 \times 10^{-5}$	$+3.532 \times 10^{-2} \pm 1.3 \times 10^{-4}$
0.975	$-2.793 \times 10^{-2} \pm 1.5 \times 10^{-5}$	$+1.181 \times 10^{-1} \pm 8.3 \times 10^{-5}$
0.999	$-2.596 \times 10^{-3} \pm 2.0 \times 10^{-6}$	$+3.140 \times 10^{-2} \pm 2.2 \times 10^{-5}$

Table 5: Coefficients of the Laurent expansion of the $f_{q\bar{q} \rightarrow t\bar{t}gg}$ function.

5. Results

We are now ready to present our numerical results for the Laurent expansions of the cross sections. We turn to dimensionless functions of the velocity β with the help of the following definition

$$\sigma_{ab \rightarrow t\bar{t}cd}^{RR}(s, m^2, \mu^2 = m^2, \alpha_s, \epsilon) = \frac{\alpha_s^4}{m^2} f_{ab \rightarrow t\bar{t}cd}(\beta, \epsilon), \quad (141)$$

where a, b are initial, and c, d final state massless partons. As shown on the left hand side above, we only give values for the case $\mu = m$, since the dependence on the scale can be obtained from renormalization group equations. The f functions admit the following expansions

$$f_{ab \rightarrow t\bar{t}cd}(\beta, \epsilon) = \sum_{i=-4}^0 \epsilon^i f_{ab \rightarrow t\bar{t}cd}^{(i)}(\beta) + \mathcal{O}(\epsilon). \quad (142)$$

We sample the functions at twenty equidistant points within the β variation range $[0, 1]$

$$\beta_i = \frac{2i-1}{40}, \quad i = 1, \dots, 20. \quad (143)$$

This is most probably sufficient to obtain a decent fitting function as has been done in the classic paper [65]. To this, we add one point very close to threshold, $\beta = 0.001$, and one very close to the infinite energy limit $\beta = 0.999$. As we will demonstrate, the study of the latter limit will require a denser sampling in the case of gluonic initial states, even though this is not immediately relevant to phenomenology due to the limited β range of current colliders producing top quarks.

β	ϵ^{-1}		ϵ^0	
0.001	$+2.947 \times 10^0$	$\pm 1.4 \times 10^{-3}$	$+5.218 \times 10^1$	$\pm 2.9 \times 10^{-2}$
0.025	$+1.196 \times 10^1$	$\pm 4.4 \times 10^{-3}$	$+1.143 \times 10^2$	$\pm 4.6 \times 10^{-2}$
0.075	$+1.293 \times 10^1$	$\pm 4.8 \times 10^{-3}$	$+8.660 \times 10^1$	$\pm 3.6 \times 10^{-2}$
0.125	$+1.127 \times 10^1$	$\pm 4.5 \times 10^{-3}$	$+5.975 \times 10^1$	$\pm 3.0 \times 10^{-2}$
0.175	$+9.161 \times 10^0$	$\pm 4.1 \times 10^{-3}$	$+3.949 \times 10^1$	$\pm 2.9 \times 10^{-2}$
0.225	$+7.062 \times 10^0$	$\pm 4.3 \times 10^{-3}$	$+2.454 \times 10^1$	$\pm 2.6 \times 10^{-2}$
0.275	$+5.149 \times 10^0$	$\pm 3.1 \times 10^{-3}$	$+1.375 \times 10^1$	$\pm 1.9 \times 10^{-2}$
0.325	$+3.469 \times 10^0$	$\pm 2.7 \times 10^{-3}$	$+6.118 \times 10^0$	$\pm 1.6 \times 10^{-2}$
0.375	$+2.063 \times 10^0$	$\pm 2.4 \times 10^{-3}$	$+9.998 \times 10^{-1}$	$\pm 1.5 \times 10^{-2}$
0.425	$+9.289 \times 10^{-1}$	$\pm 2.1 \times 10^{-3}$	-2.245×10^0	$\pm 1.3 \times 10^{-2}$
0.475	$+7.292 \times 10^{-2}$	$\pm 2.2 \times 10^{-3}$	-3.973×10^0	$\pm 1.3 \times 10^{-2}$
0.525	-5.197×10^{-1}	$\pm 2.7 \times 10^{-3}$	-4.575×10^0	$\pm 1.1 \times 10^{-2}$
0.575	-8.661×10^{-1}	$\pm 1.7 \times 10^{-3}$	-4.393×10^0	$\pm 1.1 \times 10^{-2}$
0.625	-9.995×10^{-1}	$\pm 1.6 \times 10^{-3}$	-3.711×10^0	$\pm 8.9 \times 10^{-3}$
0.675	-9.525×10^{-1}	$\pm 1.5 \times 10^{-3}$	-2.772×10^0	$\pm 8.9 \times 10^{-3}$
0.725	-7.695×10^{-1}	$\pm 1.9 \times 10^{-3}$	-1.823×10^0	$\pm 8.5 \times 10^{-3}$
0.775	-5.075×10^{-1}	$\pm 1.1 \times 10^{-3}$	-1.023×10^0	$\pm 5.6 \times 10^{-3}$
0.825	-2.310×10^{-1}	$\pm 8.5 \times 10^{-4}$	-5.028×10^{-1}	$\pm 4.5 \times 10^{-3}$
0.875	-2.577×10^{-2}	$\pm 6.8 \times 10^{-4}$	-3.085×10^{-1}	$\pm 3.5 \times 10^{-3}$
0.925	$+1.082 \times 10^{-3}$	$\pm 5.2 \times 10^{-4}$	-2.996×10^{-1}	$\pm 2.6 \times 10^{-3}$
0.975	-2.722×10^{-1}	$\pm 3.0 \times 10^{-4}$	$+2.370 \times 10^{-1}$	$\pm 1.5 \times 10^{-3}$
0.999	-2.158×10^{-1}	$\pm 1.9 \times 10^{-4}$	$+9.970 \times 10^{-1}$	$\pm 1.5 \times 10^{-3}$

Table 6: Coefficients of the Laurent expansion of the $f_{q\bar{q} \rightarrow t\bar{t}gg}$ function.

As we are interested in total cross sections at first, we use a trivial jet function equal to one. For our final results, we use a cutoff of $\Delta = 10^{-7}$. This implies a missing volume of

$$\delta\Phi_4(10^{-7}) = 8.4 \times 10^{-5} . \quad (144)$$

In order to test the independence of the results from the cutoff, we will also use a higher value of $\Delta = 10^{-6}$, which amounts to

$$\delta\Phi_4(10^{-6}) = 5.5 \times 10^{-4} . \quad (145)$$

These numbers can only be used as estimates of the relative integration errors implied by the cutoff in the non-singular case as discussed in Section 4. Nevertheless, the improvement obtained by lowering the cutoff by an order of magnitude should amount to a factor of three, which will allow us to provide realistic estimates of the quality of the final results. In fact, we will aim at a situation, in which we will be restricted by the integration error rather than by the cutoff.

For each cross section and each value of β , our simulations are performed with a total sample of 10 000 000 generated Monte Carlo events. This number is very close to the number of accepted events, since the only restriction on the phase space is given by the small cutoffs. The quality of the obtained results with this sample is discussed in the following. Nevertheless, we justify its fixed size by the purpose of this publication, which is to prove the usefulness of our approach and provide relevant numbers, while not necessarily giving the highest quality estimates. The latter exercise is left for a future publication containing complete cross sections, and not only the double-real contribution. We stress already here, that there is always a risk of underestimated errors with complicated integrands and low relative errors. Therefore, our results can probably only be trusted up to an additional factor multiplying the quoted errors. A safe bet with no special justification would be a factor of two. This is unavoidable, as practice shows, and the only way not to have to worry about the errors is to substantially increase the statistics to the point, where

the estimated precision will vastly surpass the practical requirements. This will of course be done in the mentioned future publications.

Finally, we re-stress that all computations have been performed in quadruple precision, in order to remove at least one source of concern, namely numerical instabilities. Using higher precision is by itself not yet reassuring enough, but two calculations with two different cutoffs and agreement within expectations should be.

We start our presentation with the $q\bar{q} \rightarrow t\bar{t}gg$ channel, as it contains all the complications as far as the singularity structure is concerned, but can be evaluated in a shorter time in comparison with the cutting edge $gg \rightarrow t\bar{t}gg$ process, due to the faster per phase space point computation. The results for the expansion coefficients can be found in Tabs. 5 and 6. Notice that we have not given the values for the leading singularity $1/\epsilon^4$ as it is known analytically from Section 3.2. Striking are, of course, the very large values close to threshold, which were, however, expected from the leading logarithmic behavior determined in the very same Section 3.2. At this point, we can comment on the integration errors. It is interesting that, while the relative error varies substantially, the absolute error stays more or less the same up to some factor. The reason for this behavior that we will see in all subsequent results is that the dominant, logarithmic contribution in β has much higher precision, due to simpler functional dependence (neither logarithms nor inverse square roots in the integration parameters). The remaining functional dependence is due to cancellations between contributions of the different sectors, which in turn have all more or less a similar absolute error. If we now assume that the error is a constant 2×10^{-2} (not exactly an upper bound, but rather a realistic estimator for integration with the partonic flux), we can obtain the implied relative error on the top quark pair production cross section at the TeVatron, where this channel dominates. It turns out, that the error would be 0.2%, which is more than acceptable.

Let us now study the cutoff dependence of the results. The latter is illustrated in Tab. 7, where we give the difference between the finite parts of the cross section evaluated at both cutoffs, 10^{-7} and 10^{-6} , compared to the sum of the integration errors. For many values of β , we notice that the difference is larger than the errors, albeit not by a large factor. Taking into account that we can consider the difference to be close to the actual variation with the cutoff, when changing from 10^{-6} to 10^{-7} , and that we expect a variation smaller by a factor of three, when stepping to 10^{-8} , we expect that the actual error due to finite cutoff is lower than the integration error, as certified by dividing all numbers by three and comparing to Tab. 6. The table also contains the ϵ -contribution to the two-particle phase space. We note, that it is at the level of the current integration error for most points.

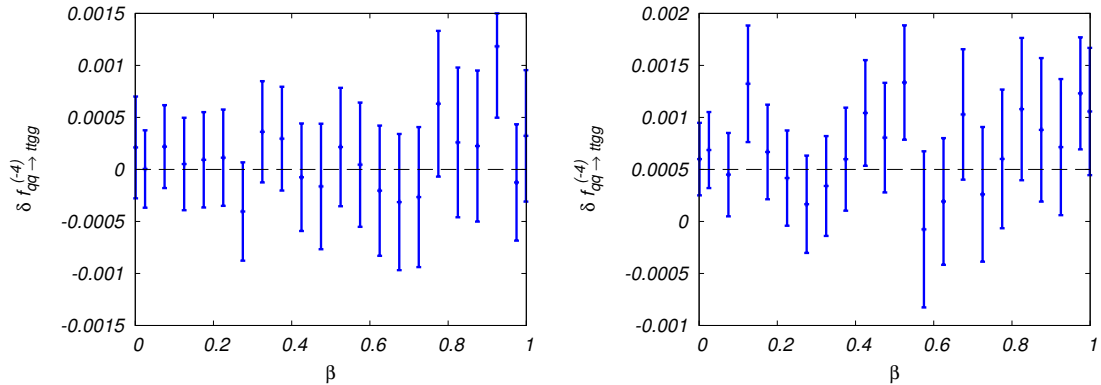


Figure 5: Difference between the value of the coefficient of the leading divergence of $f_{q\bar{q} \rightarrow t\bar{t}gg}$ obtained by numerical integration and the exact expression Eq. (97) normalized to the value of the latter. On the left panel, the lower cutoff $\Delta = 10^{-7}$ has been used, whereas on the right, $\Delta = 10^{-6}$. Notice the shifted scale on the vertical axis between the left and right panels.

β	$f^{(0)} _{10^{-7}} - f^{(0)} _{10^{-6}}$	$\Delta f^{(0)} _{10^{-7}} + \Delta f^{(0)} _{10^{-6}}$	$f^{(\epsilon, 0)}$
0.001	$+1.9 \times 10^{-2}$	4.8×10^{-2}	-3.7×10^{-8}
0.025	$+6.5 \times 10^{-2}$	8.8×10^{-2}	-3.0×10^{-5}
0.075	$+8.5 \times 10^{-2}$	7.1×10^{-2}	-3.9×10^{-4}
0.125	$+8.8 \times 10^{-2}$	6.6×10^{-2}	-1.3×10^{-3}
0.175	$+7.9 \times 10^{-2}$	5.5×10^{-2}	-2.7×10^{-3}
0.225	$+6.3 \times 10^{-2}$	4.8×10^{-2}	-4.8×10^{-3}
0.275	$+5.9 \times 10^{-2}$	3.8×10^{-2}	-6.6×10^{-3}
0.325	$+6.4 \times 10^{-2}$	3.2×10^{-2}	-9.5×10^{-3}
0.375	$+5.6 \times 10^{-2}$	3.1×10^{-2}	-1.2×10^{-2}
0.425	$+1.6 \times 10^{-2}$	2.7×10^{-2}	-1.5×10^{-2}
0.475	$+3.2 \times 10^{-2}$	2.7×10^{-2}	-1.6×10^{-2}
0.525	$+3.1 \times 10^{-2}$	2.2×10^{-2}	-1.7×10^{-2}
0.575	$+1.3 \times 10^{-2}$	2.3×10^{-2}	-1.7×10^{-2}
0.625	-1.6×10^{-4}	1.9×10^{-2}	-1.5×10^{-2}
0.675	-5.1×10^{-3}	1.6×10^{-2}	-1.0×10^{-2}
0.725	-1.5×10^{-2}	1.5×10^{-2}	-3.1×10^{-3}
0.775	-1.3×10^{-2}	1.1×10^{-2}	$+4.9 \times 10^{-3}$
0.825	-1.3×10^{-2}	8.9×10^{-3}	$+1.5 \times 10^{-2}$
0.875	-1.4×10^{-2}	7.6×10^{-3}	$+2.2 \times 10^{-2}$
0.925	-1.3×10^{-2}	5.6×10^{-3}	$+1.8 \times 10^{-2}$
0.975	-6.0×10^{-3}	3.0×10^{-3}	-3.6×10^{-2}
0.999	-2.6×10^{-3}	2.7×10^{-3}	-8.6×10^{-2}

Table 7: A comparison between the finite parts of the $f_{q\bar{q} \rightarrow t\bar{t}gg}$ function evaluated at two different values of the cutoff Δ defined in Eq. (118), $\Delta = 10^{-7}$ and $\Delta = 10^{-6}$. The second column represents the difference between the values, whereas the third the sum of the integration errors. The fourth column contains the ϵ -contribution of the two-particle phase space.

In order to check the normalization of our results, we can also compare the numerical estimate of the leading singularity, $1/\epsilon^4$, with the prediction from Section 3.2. This is done in Fig. 5 for both values of the cutoff, where we plot

$$\delta f_{q\bar{q} \rightarrow t\bar{t}gg}^{(-4)} = \frac{(4\pi)^2 f_{q\bar{q} \rightarrow t\bar{t}gg}^{(-4)} - 2C_F(C_A + 4C_F)f_{q\bar{q} \rightarrow t\bar{t}}^{(0)}}{2C_F(C_A + 4C_F)f_{q\bar{q} \rightarrow t\bar{t}}^{(0)}}, \quad (146)$$

where $f_{q\bar{q} \rightarrow t\bar{t}}^{(0)}$ is defined by the Born cross section in Appendix D. We notice that in the case of the higher cutoff, $\Delta = 10^{-6}$, the cutoff dependence is noticeable due to the tiny numerical errors. What is slightly more worrisome is that a few errors are indeed underestimated. In this case, this is due to the fact that the integration errors are very small, below permille, but the function has integrable singularities in ζ at the integration boundaries, and is thus not entirely well behaved. Based on this, we can only expect worse from the much more singular finite parts of the cross section.

Finally, in Fig. 6, we show the cross section after subtracting the leading logarithm in β . The latter would make the plot span an order of magnitude more. Notice that on the scale of this plot, the integration errors would not be noticeable.

We can, in principle, repeat the same discussion for the most complicated and computationally intensive channel, $gg \rightarrow t\bar{t}gg$. The numerical values are given in Tabs. 8 and 9, where we have again omitted the leading singularity. The essential difference to the quark annihilation channel is in the about twice larger absolute errors of the finite part for most of the β range. One can again estimate that if the error is consider constant and equal to 4×10^{-2} , then the implied uncertainty

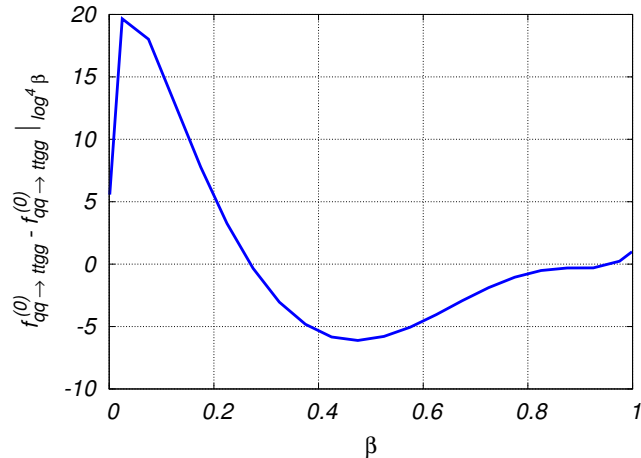


Figure 6: Finite part of $f_{q\bar{q} \rightarrow t\bar{t}gg}$ after removing the dominant logarithmic term Eq. (107).

at the LHC would be 0.4%, which is also more than acceptable. As before, we can demonstrate that the cutoff dependence is lower than the numerical integration error.

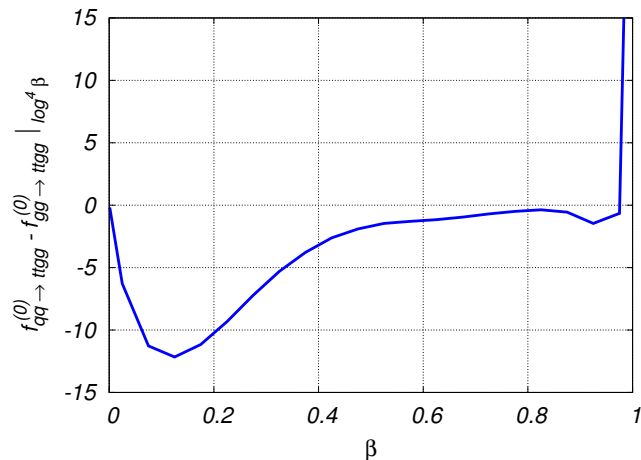


Figure 7: Finite part of $f_{gg \rightarrow t\bar{t}gg}$ after removing the dominant logarithmic term Eq. (106).

In Fig. 7, we show the finite part of the cross section after removing the dominant logarithm in β . We notice the very steep rise at the end of the range. This phenomenon is well known from the next-to-leading order cross section in the gluon fusion channel. For our numerics it has the unpleasant feature of making the calculation slightly unstable due to the extreme sensitivity to the value of β . This also points to an underestimated error at $\beta = 0.999$, anyway quoted to be rather large in Tab. 9. None of this is relevant to phenomenology at present, but we will try to get a better handle of this problem in the future.

The remaining two cross sections are much less interesting. They are less singular both in ϵ and $\log \beta$, and are moreover much smaller even after multiplication by the number of massless quark species. We give the numbers in Tabs. 10, 11, 12 and 13, and show the respective finite parts in Fig. 8.

β	ϵ^{-3}	ϵ^{-2}
0.001	$+4.534 \times 10^{-3} \pm 1.8 \times 10^{-6}$	$+1.568 \times 10^{-1} \pm 6.3 \times 10^{-5}$
0.025	$+6.086 \times 10^{-2} \pm 2.4 \times 10^{-5}$	$+1.119 \times 10^0 \pm 4.3 \times 10^{-4}$
0.075	$+1.299 \times 10^{-1} \pm 5.4 \times 10^{-5}$	$+1.664 \times 10^0 \pm 6.8 \times 10^{-4}$
0.125	$+1.776 \times 10^{-1} \pm 7.7 \times 10^{-5}$	$+1.817 \times 10^0 \pm 7.8 \times 10^{-4}$
0.175	$+2.146 \times 10^{-1} \pm 9.7 \times 10^{-5}$	$+1.836 \times 10^0 \pm 8.3 \times 10^{-4}$
0.225	$+2.451 \times 10^{-1} \pm 1.1 \times 10^{-4}$	$+1.798 \times 10^0 \pm 8.4 \times 10^{-4}$
0.275	$+2.707 \times 10^{-1} \pm 1.2 \times 10^{-4}$	$+1.727 \times 10^0 \pm 8.7 \times 10^{-4}$
0.325	$+2.918 \times 10^{-1} \pm 1.4 \times 10^{-4}$	$+1.631 \times 10^0 \pm 8.9 \times 10^{-4}$
0.375	$+3.084 \times 10^{-1} \pm 1.4 \times 10^{-4}$	$+1.516 \times 10^0 \pm 8.8 \times 10^{-4}$
0.425	$+3.191 \times 10^{-1} \pm 1.6 \times 10^{-4}$	$+1.374 \times 10^0 \pm 9.3 \times 10^{-4}$
0.475	$+3.228 \times 10^{-1} \pm 1.7 \times 10^{-4}$	$+1.204 \times 10^0 \pm 1.0 \times 10^{-3}$
0.525	$+3.175 \times 10^{-1} \pm 1.8 \times 10^{-4}$	$+1.007 \times 10^0 \pm 9.8 \times 10^{-4}$
0.575	$+3.016 \times 10^{-1} \pm 1.8 \times 10^{-4}$	$+7.777 \times 10^{-1} \pm 9.8 \times 10^{-4}$
0.625	$+2.721 \times 10^{-1} \pm 2.1 \times 10^{-4}$	$+5.218 \times 10^{-1} \pm 1.2 \times 10^{-3}$
0.675	$+2.277 \times 10^{-1} \pm 1.7 \times 10^{-4}$	$+2.543 \times 10^{-1} \pm 1.0 \times 10^{-3}$
0.725	$+1.657 \times 10^{-1} \pm 2.0 \times 10^{-4}$	$-1.360 \times 10^{-2} \pm 1.3 \times 10^{-3}$
0.775	$+8.359 \times 10^{-2} \pm 1.8 \times 10^{-4}$	$-2.575 \times 10^{-1} \pm 1.1 \times 10^{-3}$
0.825	$-2.003 \times 10^{-2} \pm 2.2 \times 10^{-4}$	$-4.275 \times 10^{-1} \pm 1.2 \times 10^{-3}$
0.875	$-1.461 \times 10^{-1} \pm 2.6 \times 10^{-4}$	$-4.536 \times 10^{-1} \pm 1.1 \times 10^{-3}$
0.925	$-2.996 \times 10^{-1} \pm 3.3 \times 10^{-4}$	$-1.805 \times 10^{-1} \pm 1.3 \times 10^{-3}$
0.975	$-4.862 \times 10^{-1} \pm 4.0 \times 10^{-4}$	$+9.458 \times 10^{-1} \pm 2.3 \times 10^{-3}$
0.999	$-5.970 \times 10^{-1} \pm 5.5 \times 10^{-4}$	$+4.118 \times 10^0 \pm 6.7 \times 10^{-3}$

Table 8: Coefficients of the Laurent expansion of the $f_{gg \rightarrow t\bar{t}gg}$ function.

6. Conclusions

The purpose of this work was to prove the usefulness of the STRIPPER approach to the problem of double-real radiation. We have considered the phenomenologically relevant case of top quark pair production, and evaluated the cross sections for the dominant channels. We have given most of the formulae needed for the implementation, and demonstrated pointwise convergence and efficiency. The immediate consequence is the possibility to evaluate the complete cross sections for top quark pair production after inclusion of the double-virtual, and real-virtual contributions. Although this requires quite some effort, we do not see any conceptual problems, unlike in the present case of double-real radiation.

We would like to point out that there are three directions of further development. First, there are many technical improvements of our implementation that can be studied. The most important are the analysis of numerical instabilities and implementation of a more efficient multi-precision library, the latter being almost trivial. Although not absolutely necessary, this work is always part of software maturation in the case of higher order calculations. The second direction involves applications to similar process, in particular removing some of the subtraction terms is sufficient to treat $e^+e^- \rightarrow t\bar{t} + X$, and $pp(\bar{p}) \rightarrow W^+W^- + X$ (and other gauge boson final states) at NNLO. The last, and probably the most interesting, direction is application of STRIPPER to final states with massless particles, such as dijet production. This requires the specification of the phase space in the case of initial and final state singularities, but as noticed in [1] involves the same treatment of the unresolved partons.

Acknowledgments

We would like to thank T. Hahn for help with FORMCALC and A. van Hameren for help with

β	ϵ^{-1}		ϵ^0	
0.001	$+3.601 \times 10^0$	$\pm 1.5 \times 10^{-3}$	$+6.175 \times 10^1$	$\pm 3.0 \times 10^{-2}$
0.025	$+1.349 \times 10^1$	$\pm 5.4 \times 10^{-3}$	$+1.197 \times 10^2$	$\pm 5.2 \times 10^{-2}$
0.075	$+1.374 \times 10^1$	$\pm 6.0 \times 10^{-3}$	$+8.129 \times 10^1$	$\pm 4.5 \times 10^{-2}$
0.125	$+1.175 \times 10^1$	$\pm 5.8 \times 10^{-3}$	$+5.280 \times 10^1$	$\pm 3.8 \times 10^{-2}$
0.175	$+9.741 \times 10^0$	$\pm 5.3 \times 10^{-3}$	$+3.461 \times 10^1$	$\pm 3.3 \times 10^{-2}$
0.225	$+8.015 \times 10^0$	$\pm 5.1 \times 10^{-3}$	$+2.300 \times 10^1$	$\pm 3.2 \times 10^{-2}$
0.275	$+6.574 \times 10^0$	$\pm 5.4 \times 10^{-3}$	$+1.557 \times 10^1$	$\pm 3.4 \times 10^{-2}$
0.325	$+5.350 \times 10^0$	$\pm 4.9 \times 10^{-3}$	$+1.062 \times 10^1$	$\pm 3.4 \times 10^{-2}$
0.375	$+4.290 \times 10^0$	$\pm 5.3 \times 10^{-3}$	$+7.186 \times 10^0$	$\pm 3.3 \times 10^{-2}$
0.425	$+3.334 \times 10^0$	$\pm 5.3 \times 10^{-3}$	$+4.774 \times 10^0$	$\pm 3.1 \times 10^{-2}$
0.475	$+2.453 \times 10^0$	$\pm 6.2 \times 10^{-3}$	$+2.944 \times 10^0$	$\pm 3.6 \times 10^{-2}$
0.525	$+1.649 \times 10^0$	$\pm 5.7 \times 10^{-3}$	$+1.595 \times 10^0$	$\pm 3.2 \times 10^{-2}$
0.575	$+8.930 \times 10^{-1}$	$\pm 5.5 \times 10^{-3}$	$+5.449 \times 10^{-1}$	$\pm 3.3 \times 10^{-2}$
0.625	$+2.321 \times 10^{-1}$	$\pm 5.6 \times 10^{-3}$	-1.188×10^{-1}	$\pm 3.4 \times 10^{-2}$
0.675	-2.740×10^{-1}	$\pm 5.6 \times 10^{-3}$	-4.124×10^{-1}	$\pm 3.5 \times 10^{-2}$
0.725	-6.121×10^{-1}	$\pm 6.9 \times 10^{-3}$	-4.498×10^{-1}	$\pm 3.6 \times 10^{-2}$
0.775	-7.540×10^{-1}	$\pm 5.6 \times 10^{-3}$	-3.971×10^{-1}	$\pm 3.5 \times 10^{-2}$
0.825	-6.363×10^{-1}	$\pm 6.3 \times 10^{-3}$	-3.371×10^{-1}	$\pm 3.9 \times 10^{-2}$
0.875	-3.241×10^{-1}	$\pm 6.0 \times 10^{-3}$	-5.518×10^{-1}	$\pm 3.7 \times 10^{-2}$
0.925	-1.076×10^{-1}	$\pm 6.3 \times 10^{-3}$	-1.462×10^0	$\pm 3.7 \times 10^{-2}$
0.975	-1.867×10^0	$\pm 9.1 \times 10^{-3}$	-6.540×10^{-1}	$\pm 4.8 \times 10^{-2}$
0.999	-1.543×10^1	$\pm 5.3 \times 10^{-2}$	$+4.437 \times 10^1$	$\pm 4.2 \times 10^{-1}$

Table 9: Coefficients of the Laurent expansion of the $f_{gg \rightarrow t\bar{t}gg}$ function.

PARNI.

This work was supported by the Heisenberg and by the Gottfried Wilhelm Leibniz programmes of the Deutsche Forschungsgemeinschaft, and by the DFG Sonderforschungsbereich/Transregio 9 ‘‘Computergestutzte Theoretische Teilchenphysik’’.

Appendix A. Collinear limits and splitting functions

In this appendix, we will reproduce the splitting functions that have been used in the derivation of the subtraction terms. The formulae are taken literally from [57] (see also [66, 67]). We start by defining the notation for the matrix elements

$$\mathcal{M}_{a_1, a_2, \dots}^{c_1, c_2, \dots; s_1, s_2, \dots}(p_1, p_2, \dots) , \quad (\text{A.1})$$

where the s_i indices stand for spin, the c_i for color, and the a_i for parton flavor. With this object, we define spin correlated amplitudes squared

$$\mathcal{T}_{a_1, \dots}^{s_1 s'_1}(p_1, \dots) \equiv \sum_{\text{spins } \neq s_1, s'_1} \sum_{\text{colors}} \mathcal{M}_{a_1, a_2, \dots}^{c_1, c_2, \dots; s_1, s_2, \dots}(p_1, p_2, \dots) \left[\mathcal{M}_{a_1, a_2, \dots}^{c_1, c_2, \dots; s'_1, s_2, \dots}(p_1, p_2, \dots) \right]^\dagger . \quad (\text{A.2})$$

Having defined the matrix elements, we now turn to next-to-leading order collinear limits of amplitudes. We first define the limits through auxiliary vectors

$$\begin{aligned} p_1^\mu &= zp^\mu + k_\perp^\mu - \frac{k_\perp^2}{z} \frac{n^\mu}{2p \cdot n} , & p_2^\mu &= (1-z)p^\mu - k_\perp^\mu - \frac{k_\perp^2}{1-z} \frac{n^\mu}{2p \cdot n} , \\ s_{12} &\equiv 2p_1 \cdot p_2 = -\frac{k_\perp^2}{z(1-z)} , & k_\perp &\rightarrow 0 , \end{aligned} \quad (\text{A.3})$$

β	ϵ^{-3}	ϵ^{-2}
0.001	$-1.452 \times 10^{-6} \pm 2.9 \times 10^{-9}$	$-1.027 \times 10^{-4} \pm 1.9 \times 10^{-7}$
0.025	$-3.627 \times 10^{-5} \pm 2.5 \times 10^{-8}$	$-1.399 \times 10^{-3} \pm 9.7 \times 10^{-7}$
0.075	$-1.096 \times 10^{-4} \pm 8.7 \times 10^{-8}$	$-3.029 \times 10^{-3} \pm 2.3 \times 10^{-6}$
0.125	$-1.853 \times 10^{-4} \pm 1.7 \times 10^{-7}$	$-4.185 \times 10^{-3} \pm 3.3 \times 10^{-6}$
0.175	$-2.644 \times 10^{-4} \pm 2.2 \times 10^{-7}$	$-5.111 \times 10^{-3} \pm 4.1 \times 10^{-6}$
0.225	$-3.486 \times 10^{-4} \pm 3.1 \times 10^{-7}$	$-5.901 \times 10^{-3} \pm 4.9 \times 10^{-6}$
0.275	$-4.377 \times 10^{-4} \pm 4.0 \times 10^{-7}$	$-6.584 \times 10^{-3} \pm 5.7 \times 10^{-6}$
0.325	$-5.323 \times 10^{-4} \pm 4.9 \times 10^{-7}$	$-7.170 \times 10^{-3} \pm 6.4 \times 10^{-6}$
0.375	$-6.322 \times 10^{-4} \pm 6.0 \times 10^{-7}$	$-7.656 \times 10^{-3} \pm 7.0 \times 10^{-6}$
0.425	$-7.362 \times 10^{-4} \pm 7.3 \times 10^{-7}$	$-8.023 \times 10^{-3} \pm 7.9 \times 10^{-6}$
0.475	$-8.422 \times 10^{-4} \pm 8.1 \times 10^{-7}$	$-8.219 \times 10^{-3} \pm 8.0 \times 10^{-6}$
0.525	$-9.468 \times 10^{-4} \pm 9.6 \times 10^{-7}$	$-8.196 \times 10^{-3} \pm 8.8 \times 10^{-6}$
0.575	$-1.045 \times 10^{-3} \pm 1.0 \times 10^{-6}$	$-7.914 \times 10^{-3} \pm 8.4 \times 10^{-6}$
0.625	$-1.136 \times 10^{-3} \pm 1.1 \times 10^{-6}$	$-7.322 \times 10^{-3} \pm 8.6 \times 10^{-6}$
0.675	$-1.208 \times 10^{-3} \pm 1.2 \times 10^{-6}$	$-6.310 \times 10^{-3} \pm 8.3 \times 10^{-6}$
0.725	$-1.256 \times 10^{-3} \pm 1.3 \times 10^{-6}$	$-4.836 \times 10^{-3} \pm 8.0 \times 10^{-6}$
0.775	$-1.264 \times 10^{-3} \pm 1.3 \times 10^{-6}$	$-2.797 \times 10^{-3} \pm 7.6 \times 10^{-6}$
0.825	$-1.222 \times 10^{-3} \pm 1.3 \times 10^{-6}$	$-8.582 \times 10^{-5} \pm 7.4 \times 10^{-6}$
0.875	$-1.107 \times 10^{-3} \pm 1.2 \times 10^{-6}$	$+3.444 \times 10^{-3} \pm 7.9 \times 10^{-6}$
0.925	$-8.799 \times 10^{-4} \pm 9.5 \times 10^{-7}$	$+8.174 \times 10^{-3} \pm 9.7 \times 10^{-6}$
0.975	$-4.551 \times 10^{-4} \pm 6.3 \times 10^{-7}$	$+1.546 \times 10^{-2} \pm 1.3 \times 10^{-5}$
0.999	$-3.921 \times 10^{-5} \pm 5.9 \times 10^{-7}$	$+2.366 \times 10^{-2} \pm 1.9 \times 10^{-5}$

Table 10: Coefficients of the Laurent expansion of the $f_{gg \rightarrow t\bar{t}q\bar{q}}$ function.

where $p^2 = n^2 = p \cdot k_\perp = n \cdot k_\perp = 0$. Notice that all vectors here and below are outgoing. The case we are interested in, namely some of the vectors being in-going, is recovered by crossing. In the above collinear limit, the matrix element factorizes as follows

$$|\mathcal{M}_{a_1, a_2, \dots}(p_1, p_2, \dots)|^2 \simeq \frac{2}{s_{12}} 4\pi\mu^{2\epsilon} \alpha_s \mathcal{T}_{a, \dots}^{ss'}(p, \dots) \hat{P}_{a_1 a_2}^{ss'}(z, k_\perp; \epsilon) . \quad (\text{A.4})$$

The splitting functions $\hat{P}_{a_1 a_2}^{ss'}$ depend on the parton flavors. For the general case

$$a(p) \rightarrow a_1(zp + k_\perp + \mathcal{O}(k_\perp^2)) + a_2((1-z)p - k_\perp + \mathcal{O}(k_\perp^2)) , \quad (\text{A.5})$$

they read

$$\hat{P}_{qg}^{ss'}(z, k_\perp; \epsilon) = \hat{P}_{gq}^{ss'}(z, k_\perp; \epsilon) = \delta_{ss'} C_F \left[\frac{1+z^2}{1-z} - \epsilon(1-z) \right] , \quad (\text{A.6})$$

$$\hat{P}_{gq}^{ss'}(z, k_\perp; \epsilon) = \hat{P}_{qg}^{ss'}(z, k_\perp; \epsilon) = \delta_{ss'} C_F \left[\frac{1+(1-z)^2}{z} - \epsilon z \right] , \quad (\text{A.7})$$

$$\hat{P}_{q\bar{q}}^{\mu\nu}(z, k_\perp; \epsilon) = \hat{P}_{\bar{q}q}^{\mu\nu}(z, k_\perp; \epsilon) = T_F \left[-g^{\mu\nu} + 4z(1-z) \frac{k_\perp^\mu k_\perp^\nu}{k_\perp^2} \right] , \quad (\text{A.8})$$

$$\hat{P}_{g\bar{g}}^{\mu\nu}(z, k_\perp; \epsilon) = 2C_A \left[-g^{\mu\nu} \left(\frac{z}{1-z} + \frac{1-z}{z} \right) - 2(1-\epsilon)z(1-z) \frac{k_\perp^\mu k_\perp^\nu}{k_\perp^2} \right] . \quad (\text{A.9})$$

β	ϵ^{-1}	ϵ^0
0.001	$-3.622 \times 10^{-3} \pm 6.2 \times 10^{-6}$	$-8.500 \times 10^{-2} \pm 1.8 \times 10^{-4}$
0.025	$-2.672 \times 10^{-2} \pm 1.9 \times 10^{-5}$	$-3.366 \times 10^{-1} \pm 2.7 \times 10^{-4}$
0.075	$-4.108 \times 10^{-2} \pm 3.2 \times 10^{-5}$	$-3.636 \times 10^{-1} \pm 3.4 \times 10^{-4}$
0.125	$-4.604 \times 10^{-2} \pm 4.1 \times 10^{-5}$	$-3.275 \times 10^{-1} \pm 4.4 \times 10^{-4}$
0.175	$-4.781 \times 10^{-2} \pm 4.3 \times 10^{-5}$	$-2.869 \times 10^{-1} \pm 3.7 \times 10^{-4}$
0.225	$-4.806 \times 10^{-2} \pm 4.6 \times 10^{-5}$	$-2.495 \times 10^{-1} \pm 3.7 \times 10^{-4}$
0.275	$-4.742 \times 10^{-2} \pm 4.8 \times 10^{-5}$	$-2.173 \times 10^{-1} \pm 3.5 \times 10^{-4}$
0.325	$-4.607 \times 10^{-2} \pm 5.0 \times 10^{-5}$	$-1.881 \times 10^{-1} \pm 3.6 \times 10^{-4}$
0.375	$-4.404 \times 10^{-2} \pm 5.2 \times 10^{-5}$	$-1.612 \times 10^{-1} \pm 3.5 \times 10^{-4}$
0.425	$-4.137 \times 10^{-2} \pm 5.5 \times 10^{-5}$	$-1.364 \times 10^{-1} \pm 3.6 \times 10^{-4}$
0.475	$-3.770 \times 10^{-2} \pm 5.3 \times 10^{-5}$	$-1.111 \times 10^{-1} \pm 3.5 \times 10^{-4}$
0.525	$-3.296 \times 10^{-2} \pm 5.7 \times 10^{-5}$	$-8.534 \times 10^{-2} \pm 3.8 \times 10^{-4}$
0.575	$-2.716 \times 10^{-2} \pm 5.9 \times 10^{-5}$	$-5.918 \times 10^{-2} \pm 3.7 \times 10^{-4}$
0.625	$-2.032 \times 10^{-2} \pm 5.8 \times 10^{-5}$	$-3.295 \times 10^{-2} \pm 4.0 \times 10^{-4}$
0.675	$-1.234 \times 10^{-2} \pm 5.7 \times 10^{-5}$	$-7.767 \times 10^{-3} \pm 3.7 \times 10^{-4}$
0.725	$-3.706 \times 10^{-3} \pm 5.2 \times 10^{-5}$	$+1.446 \times 10^{-2} \pm 3.3 \times 10^{-4}$
0.775	$+5.117 \times 10^{-3} \pm 5.0 \times 10^{-5}$	$+3.236 \times 10^{-2} \pm 3.1 \times 10^{-4}$
0.825	$+1.331 \times 10^{-2} \pm 5.6 \times 10^{-5}$	$+4.375 \times 10^{-2} \pm 2.9 \times 10^{-4}$
0.875	$+1.891 \times 10^{-2} \pm 7.8 \times 10^{-5}$	$+4.700 \times 10^{-2} \pm 2.9 \times 10^{-4}$
0.925	$+1.833 \times 10^{-2} \pm 4.4 \times 10^{-5}$	$+4.423 \times 10^{-2} \pm 2.4 \times 10^{-4}$
0.975	$-3.231 \times 10^{-3} \pm 6.0 \times 10^{-5}$	$+6.853 \times 10^{-2} \pm 2.6 \times 10^{-4}$
0.999	$-6.995 \times 10^{-2} \pm 1.9 \times 10^{-4}$	$+3.312 \times 10^{-1} \pm 1.2 \times 10^{-3}$

Table 11: Coefficients of the Laurent expansion of the $f_{gg \rightarrow t\bar{t}q\bar{q}}$ function.

Let us now turn to the more complicated case of triple-collinear limits. Consider the set of three vectors

$$p_i^\mu = x_i p^\mu + k_{\perp i}^\mu - \frac{k_{\perp i}^2}{x_i} \frac{n^\mu}{2p \cdot n}, \quad i = 1, 2, 3, \quad (\text{A.10})$$

where as before $p^2 = n^2 = p \cdot k_{\perp i} = n \cdot k_{\perp i} = 0$. This configuration fulfills no other constraints, but rather the limits are expressed through derived variables

$$z_i = \frac{x_i}{\sum_{j=1}^3 x_j}, \quad (\text{A.11})$$

$$\tilde{k}_i^\mu = k_{\perp i}^\mu - \frac{x_i}{\sum_{k=1}^3 x_k} \sum_{j=1}^3 k_{\perp j}^\mu. \quad (\text{A.12})$$

We also define

$$t_{ij,k} \equiv 2 \frac{z_i s_{jk} - z_j s_{ik}}{z_i + z_j} + \frac{z_i - z_j}{z_i + z_j} s_{ij}, \quad (\text{A.13})$$

with $s_{ij} = (p_i + p_j)^2$.

The factorization formula is now

$$|\mathcal{M}_{a_1, a_2, a_3, \dots}(p_1, p_2, p_3, \dots)|^2 \simeq \left(\frac{8\pi\mu^{2\epsilon}\alpha_s}{s_{123}} \right)^2 \mathcal{T}_{a, \dots}^{ss'}(xp, \dots) \hat{P}_{a_1 a_2 a_3}^{ss'}, \quad (\text{A.14})$$

with $s_{123} = (p_1 + p_2 + p_3)^2$ and $x = x_1 + x_2 + x_3$.

β	ϵ^{-3}	ϵ^{-2}
0.001	$-1.962 \times 10^{-6} \pm 8.8 \times 10^{-10}$	$-1.418 \times 10^{-4} \pm 6.5 \times 10^{-8}$
0.025	$-4.907 \times 10^{-5} \pm 2.4 \times 10^{-8}$	$-1.967 \times 10^{-3} \pm 9.6 \times 10^{-7}$
0.075	$-1.464 \times 10^{-4} \pm 1.4 \times 10^{-7}$	$-4.255 \times 10^{-3} \pm 2.5 \times 10^{-6}$
0.125	$-2.406 \times 10^{-4} \pm 1.4 \times 10^{-7}$	$-5.749 \times 10^{-3} \pm 3.1 \times 10^{-6}$
0.175	$-3.297 \times 10^{-4} \pm 1.9 \times 10^{-7}$	$-6.740 \times 10^{-3} \pm 3.7 \times 10^{-6}$
0.225	$-4.129 \times 10^{-4} \pm 2.5 \times 10^{-7}$	$-7.342 \times 10^{-3} \pm 4.2 \times 10^{-6}$
0.275	$-4.866 \times 10^{-4} \pm 3.0 \times 10^{-7}$	$-7.593 \times 10^{-3} \pm 4.5 \times 10^{-6}$
0.325	$-5.508 \times 10^{-4} \pm 3.4 \times 10^{-7}$	$-7.558 \times 10^{-3} \pm 4.7 \times 10^{-6}$
0.375	$-6.029 \times 10^{-4} \pm 3.9 \times 10^{-7}$	$-7.250 \times 10^{-3} \pm 4.7 \times 10^{-6}$
0.425	$-6.429 \times 10^{-4} \pm 4.2 \times 10^{-7}$	$-6.723 \times 10^{-3} \pm 4.7 \times 10^{-6}$
0.475	$-6.682 \times 10^{-4} \pm 4.5 \times 10^{-7}$	$-5.998 \times 10^{-3} \pm 4.3 \times 10^{-6}$
0.525	$-6.783 \times 10^{-4} \pm 4.6 \times 10^{-7}$	$-5.117 \times 10^{-3} \pm 4.0 \times 10^{-6}$
0.575	$-6.724 \times 10^{-4} \pm 4.5 \times 10^{-7}$	$-4.113 \times 10^{-3} \pm 3.5 \times 10^{-6}$
0.625	$-6.503 \times 10^{-4} \pm 4.4 \times 10^{-7}$	$-3.037 \times 10^{-3} \pm 3.1 \times 10^{-6}$
0.675	$-6.124 \times 10^{-4} \pm 4.2 \times 10^{-7}$	$-1.945 \times 10^{-3} \pm 2.6 \times 10^{-6}$
0.725	$-5.569 \times 10^{-4} \pm 3.9 \times 10^{-7}$	$-8.748 \times 10^{-4} \pm 2.2 \times 10^{-6}$
0.775	$-4.869 \times 10^{-4} \pm 3.6 \times 10^{-7}$	$+9.961 \times 10^{-5} \pm 2.0 \times 10^{-6}$
0.825	$-4.001 \times 10^{-4} \pm 3.1 \times 10^{-7}$	$+9.114 \times 10^{-4} \pm 1.7 \times 10^{-6}$
0.875	$-2.998 \times 10^{-4} \pm 2.4 \times 10^{-7}$	$+1.461 \times 10^{-3} \pm 1.5 \times 10^{-6}$
0.925	$-1.874 \times 10^{-4} \pm 1.5 \times 10^{-7}$	$+1.609 \times 10^{-3} \pm 1.3 \times 10^{-6}$
0.975	$-6.459 \times 10^{-5} \pm 4.3 \times 10^{-8}$	$+1.052 \times 10^{-3} \pm 6.0 \times 10^{-7}$
0.999	$-2.617 \times 10^{-6} \pm 2.0 \times 10^{-9}$	$+1.013 \times 10^{-4} \pm 1.1 \times 10^{-7}$

Table 12: Coefficients of the Laurent expansion of the $f_{q\bar{q} \rightarrow t\bar{t}q'\bar{q}'}$ function.

The complete set of splitting functions is (in the case of spin conservation, we give only the spin averaged splitting functions $\langle \hat{P}_{a_1 a_2 a_3} \rangle$)

$$\langle \hat{P}_{\bar{q}_1' q_2' q_3} \rangle = \frac{1}{2} C_F T_F \frac{s_{123}}{s_{12}} \left[-\frac{t_{12,3}^2}{s_{12} s_{123}} + \frac{4z_3 + (z_1 - z_2)^2}{z_1 + z_2} + (1 - 2\epsilon) \left(z_1 + z_2 - \frac{s_{12}}{s_{123}} \right) \right] . \quad (\text{A.15})$$

Notice that we have omitted the case of identical quarks, which is not needed in the present paper. The splitting functions for this case can be found in [57]. The remaining functions are

$$\langle \hat{P}_{g_1 g_2 q_3} \rangle = C_F^2 \langle \hat{P}_{g_1 g_2 q_3}^{(\text{ab})} \rangle + C_F C_A \langle \hat{P}_{g_1 g_2 q_3}^{(\text{nab})} \rangle , \quad (\text{A.16})$$

with

$$\begin{aligned} \langle \hat{P}_{g_1 g_2 q_3}^{(\text{ab})} \rangle &= \left\{ \frac{s_{123}^2}{2s_{13}s_{23}} z_3 \left[\frac{1+z_3^2}{z_1 z_2} - \epsilon \frac{z_1^2+z_2^2}{z_1 z_2} - \epsilon(1+\epsilon) \right] \right. \\ &+ \frac{s_{123}}{s_{13}} \left[\frac{z_3(1-z_1) + (1-z_2)^3}{z_1 z_2} + \epsilon^2(1+z_3) - \epsilon(z_1^2 + z_1 z_2 + z_2^2) \frac{1-z_2}{z_1 z_2} \right] \\ &\left. + (1-\epsilon) \left[\epsilon - (1-\epsilon) \frac{s_{23}}{s_{13}} \right] \right\} + (1 \leftrightarrow 2) , \quad (\text{A.17}) \end{aligned}$$

β	ϵ^{-1}	ϵ^0
0.001	$-5.122 \times 10^{-3} \pm 2.4 \times 10^{-6}$	$-1.232 \times 10^{-1} \pm 6.2 \times 10^{-5}$
0.025	$-3.933 \times 10^{-2} \pm 2.0 \times 10^{-5}$	$-5.229 \times 10^{-1} \pm 2.9 \times 10^{-4}$
0.075	$-6.148 \times 10^{-2} \pm 3.6 \times 10^{-5}$	$-5.894 \times 10^{-1} \pm 6.4 \times 10^{-4}$
0.125	$-6.810 \times 10^{-2} \pm 3.9 \times 10^{-5}$	$-5.340 \times 10^{-1} \pm 4.0 \times 10^{-4}$
0.175	$-6.802 \times 10^{-2} \pm 4.1 \times 10^{-5}$	$-4.529 \times 10^{-1} \pm 3.6 \times 10^{-4}$
0.225	$-6.408 \times 10^{-2} \pm 4.1 \times 10^{-5}$	$-3.670 \times 10^{-1} \pm 3.5 \times 10^{-4}$
0.275	$-5.768 \times 10^{-2} \pm 4.3 \times 10^{-5}$	$-2.848 \times 10^{-1} \pm 3.8 \times 10^{-4}$
0.325	$-4.992 \times 10^{-2} \pm 3.7 \times 10^{-5}$	$-2.112 \times 10^{-1} \pm 2.6 \times 10^{-4}$
0.375	$-4.117 \times 10^{-2} \pm 3.7 \times 10^{-5}$	$-1.453 \times 10^{-1} \pm 2.4 \times 10^{-4}$
0.425	$-3.225 \times 10^{-2} \pm 3.8 \times 10^{-5}$	$-9.050 \times 10^{-2} \pm 3.4 \times 10^{-4}$
0.475	$-2.344 \times 10^{-2} \pm 2.7 \times 10^{-5}$	$-4.580 \times 10^{-2} \pm 1.7 \times 10^{-4}$
0.525	$-1.523 \times 10^{-2} \pm 2.9 \times 10^{-5}$	$-1.203 \times 10^{-2} \pm 2.9 \times 10^{-4}$
0.575	$-7.844 \times 10^{-3} \pm 2.6 \times 10^{-5}$	$+1.230 \times 10^{-2} \pm 1.7 \times 10^{-4}$
0.625	$-1.715 \times 10^{-3} \pm 2.1 \times 10^{-5}$	$+2.634 \times 10^{-2} \pm 1.6 \times 10^{-4}$
0.675	$+2.967 \times 10^{-3} \pm 2.0 \times 10^{-5}$	$+3.260 \times 10^{-2} \pm 1.1 \times 10^{-4}$
0.725	$+5.959 \times 10^{-3} \pm 1.4 \times 10^{-5}$	$+3.152 \times 10^{-2} \pm 8.3 \times 10^{-5}$
0.775	$+7.193 \times 10^{-3} \pm 1.3 \times 10^{-5}$	$+2.558 \times 10^{-2} \pm 9.4 \times 10^{-5}$
0.825	$+6.576 \times 10^{-3} \pm 1.2 \times 10^{-5}$	$+1.680 \times 10^{-2} \pm 6.1 \times 10^{-5}$
0.875	$+4.164 \times 10^{-3} \pm 7.8 \times 10^{-6}$	$+8.379 \times 10^{-3} \pm 4.3 \times 10^{-5}$
0.925	$+3.782 \times 10^{-4} \pm 8.4 \times 10^{-6}$	$+3.761 \times 10^{-3} \pm 4.1 \times 10^{-4}$
0.975	$-3.322 \times 10^{-3} \pm 2.9 \times 10^{-6}$	$+9.508 \times 10^{-3} \pm 1.3 \times 10^{-5}$
0.999	$-1.074 \times 10^{-3} \pm 8.8 \times 10^{-7}$	$+7.280 \times 10^{-3} \pm 7.3 \times 10^{-6}$

Table 13: Coefficients of the Laurent expansion of the $f_{q\bar{q} \rightarrow t\bar{t}q'\bar{q}'}$ function.

$$\begin{aligned}
\langle \hat{P}_{g_1 g_2 q_3}^{(\text{nab})} \rangle &= \left\{ (1-\epsilon) \left(\frac{t_{12,3}^2}{4s_{12}^2} + \frac{1}{4} - \frac{\epsilon}{2} \right) + \frac{s_{123}^2}{2s_{12}s_{13}} \left[\frac{(1-z_3)^2(1-\epsilon) + 2z_3}{z_2} \right. \right. \\
&+ \left. \frac{z_2^2(1-\epsilon) + 2(1-z_2)}{1-z_3} \right] - \frac{s_{123}^2}{4s_{13}s_{23}} z_3 \left[\frac{(1-z_3)^2(1-\epsilon) + 2z_3}{z_1 z_2} + \epsilon(1-\epsilon) \right] \\
&+ \frac{s_{123}}{2s_{12}} \left[(1-\epsilon) \frac{z_1(2-2z_1+z_1^2) - z_2(6-6z_2+z_2^2)}{z_2(1-z_3)} + 2\epsilon \frac{z_3(z_1-2z_2)-z_2}{z_2(1-z_3)} \right] \\
&+ \frac{s_{123}}{2s_{13}} \left[(1-\epsilon) \frac{(1-z_2)^3 + z_3^2 - z_2}{z_2(1-z_3)} - \epsilon \left(\frac{2(1-z_2)(z_2-z_3)}{z_2(1-z_3)} - z_1 + z_2 \right) \right. \\
&\left. - \frac{z_3(1-z_1) + (1-z_2)^3}{z_1 z_2} + \epsilon(1-z_2) \left(\frac{z_1^2 + z_2^2}{z_1 z_2} - \epsilon \right) \right] \Big\} + (1 \leftrightarrow 2) . \quad (\text{A.18})
\end{aligned}$$

Similarly

$$\hat{P}_{g_1 q_2 \bar{q}_3}^{\mu\nu} = C_F T_F \hat{P}_{g_1 q_2 \bar{q}_3}^{\mu\nu(\text{ab})} + C_A T_F \hat{P}_{g_1 q_2 \bar{q}_3}^{\mu\nu(\text{nab})} , \quad (\text{A.19})$$

with

$$\begin{aligned}
\hat{P}_{g_1 q_2 \bar{q}_3}^{\mu\nu(\text{ab})} &= -g^{\mu\nu} \left[-2 + \frac{2s_{123}s_{23} + (1-\epsilon)(s_{123} - s_{23})^2}{s_{12}s_{13}} \right] \\
&+ \frac{4s_{123}}{s_{12}s_{13}} \left(\tilde{k}_3^\mu \tilde{k}_2^\nu + \tilde{k}_2^\mu \tilde{k}_3^\nu - (1-\epsilon) \tilde{k}_1^\mu \tilde{k}_1^\nu \right) , \quad (\text{A.20})
\end{aligned}$$

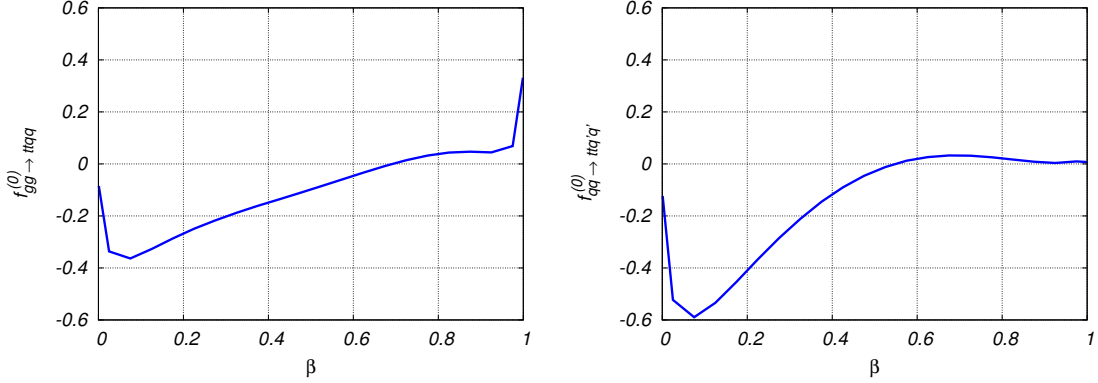


Figure 8: Finite parts of $f_{gg \rightarrow t\bar{t}q\bar{q}}$ (left) and $f_{q\bar{q} \rightarrow t\bar{t}q'\bar{q}'}$ (right).

$$\begin{aligned}
\hat{P}_{g_1 g_2 g_3}^{\mu\nu (\text{nab})} &= \frac{1}{4} \left\{ \frac{s_{123}}{s_{23}^2} \left[g^{\mu\nu} \frac{t_{23,1}^2}{s_{123}} - 16 \frac{z_2^2 z_3^2}{z_1(1-z_1)} \left(\frac{\tilde{k}_2}{z_2} - \frac{\tilde{k}_3}{z_3} \right)^\mu \left(\frac{\tilde{k}_2}{z_2} - \frac{\tilde{k}_3}{z_3} \right)^\nu \right] \right. \\
&+ \frac{s_{123}}{s_{12}s_{13}} \left[2s_{123}g^{\mu\nu} - 4(\tilde{k}_2^\mu \tilde{k}_3^\nu + \tilde{k}_3^\mu \tilde{k}_2^\nu - (1-\epsilon)\tilde{k}_1^\mu \tilde{k}_1^\nu) \right] \\
&- g^{\mu\nu} \left[-(1-2\epsilon) + 2\frac{s_{123}}{s_{12}} \frac{1-z_3}{z_1(1-z_1)} + 2\frac{s_{123}}{s_{23}} \frac{1-z_1+2z_1^2}{z_1(1-z_1)} \right] \\
&+ \frac{s_{123}}{s_{12}s_{23}} \left[-2s_{123}g^{\mu\nu} \frac{z_2(1-2z_1)}{z_1(1-z_1)} - 16\tilde{k}_3^\mu \tilde{k}_3^\nu \frac{z_2^2}{z_1(1-z_1)} + 8(1-\epsilon)\tilde{k}_2^\mu \tilde{k}_2^\nu \right. \\
&\left. + 4(\tilde{k}_2^\mu \tilde{k}_3^\nu + \tilde{k}_3^\mu \tilde{k}_2^\nu) \left(\frac{2z_2(z_3-z_1)}{z_1(1-z_1)} + (1-\epsilon) \right) \right] \left. \right\} + (2 \leftrightarrow 3) . \quad (\text{A.21})
\end{aligned}$$

Finally

$$\begin{aligned}
\hat{P}_{g_1 g_2 g_3}^{\mu\nu} &= C_A^2 \left\{ \frac{(1-\epsilon)}{4s_{12}^2} \left[-g^{\mu\nu} t_{12,3}^2 + 16s_{123} \frac{z_1^2 z_2^2}{z_3(1-z_3)} \left(\frac{\tilde{k}_2}{z_2} - \frac{\tilde{k}_1}{z_1} \right)^\mu \left(\frac{\tilde{k}_2}{z_2} - \frac{\tilde{k}_1}{z_1} \right)^\nu \right] \right. \\
&- \frac{3}{4}(1-\epsilon)g^{\mu\nu} + \frac{s_{123}}{s_{12}} g^{\mu\nu} \frac{1}{z_3} \left[\frac{2(1-z_3)+4z_3^2}{1-z_3} - \frac{1-2z_3(1-z_3)}{z_1(1-z_1)} \right] \\
&+ \frac{s_{123}(1-\epsilon)}{s_{12}s_{13}} \left[2z_1 \left(\frac{\tilde{k}_2^\mu \tilde{k}_2^\nu}{z_3(1-z_3)} + \frac{\tilde{k}_3^\mu \tilde{k}_3^\nu}{z_2(1-z_2)} \right) \right. \\
&+ \frac{s_{123}}{2(1-\epsilon)} g^{\mu\nu} \left(\frac{4z_2 z_3 + 2z_1(1-z_1) - 1}{(1-z_2)(1-z_3)} - \frac{1-2z_1(1-z_1)}{z_2 z_3} \right) \\
&\left. + \left(\tilde{k}_2^\mu \tilde{k}_3^\nu + \tilde{k}_3^\mu \tilde{k}_2^\nu \right) \left(\frac{2z_2(1-z_2)}{z_3(1-z_3)} - 3 \right) \right] \left. \right\} + (5 \text{ permutations}) . \quad (\text{A.22})
\end{aligned}$$

Appendix B. Soft limits in the presence of massive partons

While Ref. [57] contains a summary of the behavior of QCD matrix elements in singular limits at next-to-next-to-leading order, the authors restricted themselves to the case of massless partons. Since massive partons do not induce collinear singularities, we need only consider the soft limit. It is well known that the eikonal current has the same form in both massless and massive cases.

This implies that as long as we describe strongly ordered limits, no modification of the expressions is needed. Surprisingly, one observes a difference in the double-soft limit, in which the energies of both gluons (there is nothing special in the case of a soft quark pair) vanish at the same rate. To be more specific, we shall consider two gluons with momenta q_1 and q_2 , which are rescaled by a factor λ

$$q_1 \rightarrow \lambda q_1, \quad q_2 \rightarrow \lambda q_2, \quad (\text{B.1})$$

and we will study the limit $\lambda \rightarrow 0$. As explained in [57], the matrix element factorizes as follows

$$\langle a_1, a_2; \mu_1, \mu_2 | \mathcal{M}_{g,g,c_1,\dots,c_n}(q_1, q_2, p_1, \dots, p_n) \rangle \simeq g^2 \mu^{2\epsilon} J_{\mu_1 \mu_2}^{a_1 a_2}(q_1, q_2) | \mathcal{M}_{c_1, \dots, c_n}(p_1, \dots, p_n) \rangle, \quad (\text{B.2})$$

where g is the strong coupling constant, μ the dimension unit in dimensional regularization (introduced through the explicit dependence in the coupling constant), and the two-gluon soft current $J_{\mu_1 \mu_2}^{a_1 a_2}(q_1, q_2)$ is given by

$$\begin{aligned} J_{a_1 a_2}^{\mu_1 \mu_2}(q_1, q_2) &= \frac{1}{2} \{ J_{a_1}^{\mu_1}(q_1), J_{a_2}^{\mu_2}(q_2) \} + i f_{a_1 a_2 a_3} \sum_{i=1}^n T_i^{a_3} \left\{ \frac{p_i^{\mu_1} q_1^{\mu_2} - p_i^{\mu_2} q_2^{\mu_1}}{(q_1 \cdot q_2) [p_i \cdot (q_1 + q_2)]} \right. \\ &\quad \left. - \frac{p_i \cdot (q_1 - q_2)}{2 [p_i \cdot (q_1 + q_2)]} \left[\frac{p_i^{\mu_1} p_i^{\mu_2}}{(p_i \cdot q_1)(p_i \cdot q_2)} + \frac{g^{\mu_1 \mu_2}}{q_1 \cdot q_2} \right] \right\}, \end{aligned} \quad (\text{B.3})$$

with the eikonal current defined as

$$\mathbf{J}^\mu(q) = \sum_{i=1}^n \mathbf{T}_i \frac{p_i^\mu}{p_i \cdot q}. \quad (\text{B.4})$$

The algebra of the colour operators \mathbf{T}_i has been discussed at length in [2]. The expression Eq. (B.3) is as in [57] and can be derived by taking into account all diagrams with the two soft gluons attached to a hard parton line through an eikonal coupling. The triple gluon vertex has to be treated exactly, since all momenta are of the same order. The chosen class of diagrams is shown to be sufficient by power counting in a physical gauge. Moreover, contraction with physical polarization vectors has been used to eliminate terms proportional to the soft gluon momentum.

The difference between massive and massless cases occurs, when squaring the matrix element. The factorization formula then contains the factor

$$[J_{\mu\nu}^{a_1 a_2}(q_1, q_2)]^\dagger d^{\mu\sigma}(q_1) d^{\nu\rho}(q_2) J_{\sigma\rho}^{a_1 a_2}(q_1, q_2) = \frac{1}{2} \{ \mathbf{J}^2(q_1), \mathbf{J}^2(q_2) \} - C_A \sum_{i,j=1}^n \mathbf{T}_i \cdot \mathbf{T}_j \mathcal{S}_{ij}(q_1, q_2) + \dots, \quad (\text{B.5})$$

where $d^{\mu\nu}(q)$ is the polarization tensor obtained by summing over gluon polarizations. Due to current conservation, we can make the replacement $d^{\mu\nu}(q) \rightarrow -g^{\mu\nu}$. The terms vanishing when acting on a physical matrix element are denoted by the dots at the end of the above equation.

In order to recast what is essentially the square of the two-gluon current in Eq. (B.3) into the form of the right hand side of Eq. (B.5), some colour algebra is needed (rightfully called ‘‘quite cumbersome’’ by the authors of [57]). The process is simplified substantially by the use of the following two identities

$$i f^{a_1 a_2 a_3} [\{T_i^{a_1}, T_j^{a_2}\}, T_k^{a_3}] = 2C_A \mathbf{T}_i \cdot \mathbf{T}_j (\delta_{ik} - \delta_{jk}); \quad (\text{B.6})$$

$$\begin{aligned} &\{ \{T_i^{a_1}, T_j^{a_2}\}, \{T_k^{a_1}, T_l^{a_2}\} \} + \{ \{T_i^{a_1}, T_l^{a_2}\}, \{T_k^{a_1}, T_j^{a_2}\} \} \\ &= 8 \{ \mathbf{T}_i \cdot \mathbf{T}_k, \mathbf{T}_j \cdot \mathbf{T}_l \} + 2C_A \left[3\delta_{il}\delta_{jk} \mathbf{T}_i \cdot \mathbf{T}_j + 3\delta_{ij}\delta_{kl} \mathbf{T}_i \cdot \mathbf{T}_k \right. \\ &\quad \left. - 2\delta_{ij}\delta_{jk} \mathbf{T}_i \cdot \mathbf{T}_l - 2\delta_{ij}\delta_{jl} \mathbf{T}_i \cdot \mathbf{T}_k - 2(\delta_{ik}\delta_{kl} + \delta_{jk}\delta_{kl}) \mathbf{T}_i \cdot \mathbf{T}_j \right]. \end{aligned}$$

The result for the $\mathcal{S}_{ij}(q_1, q_2)$ function can be split into two parts

$$\mathcal{S}_{ij}(q_1, q_2) = \mathcal{S}_{ij}^{m=0}(q_1, q_2) + \left(m_i^2 \mathcal{S}_{ij}^{m \neq 0}(q_1, q_2) + m_j^2 \mathcal{S}_{ji}^{m \neq 0}(q_1, q_2) \right), \quad (\text{B.7})$$

where the first term has already been given in [57] and reads

$$\begin{aligned} \mathcal{S}_{ij}^{m=0}(q_1, q_2) &= \frac{(1-\epsilon)}{(q_1 \cdot q_2)^2} \frac{p_i \cdot q_1 p_j \cdot q_2 + p_i \cdot q_2 p_j \cdot q_1}{p_i \cdot (q_1 + q_2) p_j \cdot (q_1 + q_2)} \\ &\quad - \frac{(p_i \cdot p_j)^2}{2 p_i \cdot q_1 p_j \cdot q_2 p_i \cdot q_2 p_j \cdot q_1} \left[2 - \frac{p_i \cdot q_1 p_j \cdot q_2 + p_i \cdot q_2 p_j \cdot q_1}{p_i \cdot (q_1 + q_2) p_j \cdot (q_1 + q_2)} \right] \\ &\quad + \frac{p_i \cdot p_j}{2 q_1 \cdot q_2} \left[\frac{2}{p_i \cdot q_1 p_j \cdot q_2} + \frac{2}{p_j \cdot q_1 p_i \cdot q_2} - \frac{1}{p_i \cdot (q_1 + q_2) p_j \cdot (q_1 + q_2)} \right] \\ &\quad \times \left(4 + \frac{(p_i \cdot q_1 p_j \cdot q_2 + p_i \cdot q_2 p_j \cdot q_1)^2}{p_i \cdot q_1 p_j \cdot q_2 p_i \cdot q_2 p_j \cdot q_1} \right). \end{aligned} \quad (\text{B.8})$$

The second contribution in Eq. (B.7) is new and represents the additional terms generated by non-vanishing masses. The relevant function is

$$\begin{aligned} \mathcal{S}_{ij}^{m \neq 0}(q_1, q_2) &= -\frac{1}{4 q_1 \cdot q_2 p_i \cdot q_1 p_i \cdot q_2} + \frac{p_i \cdot p_j p_j \cdot (q_1 + q_2)}{2 p_i \cdot q_1 p_j \cdot q_2 p_i \cdot q_2 p_j \cdot q_1 p_i \cdot (q_1 + q_2)} \\ &\quad - \frac{1}{2 q_1 \cdot q_2 p_i \cdot (q_1 + q_2) p_j \cdot (q_1 + q_2)} \left(\frac{(p_j \cdot q_1)^2}{p_i \cdot q_1 p_j \cdot q_2} + \frac{(p_j \cdot q_2)^2}{p_i \cdot q_2 p_j \cdot q_1} \right). \end{aligned} \quad (\text{B.9})$$

Appendix C. Collinear behavior in the double-soft limit

Due to the particular phase space decomposition introduced in [1], the singular matrix element limits that need to be considered in the construction of the subtraction terms, are covered directly by the formulae from [57] (aside from the modification given in the previous appendix for the case of massive partons). Nevertheless, one case turns out to be slightly inconvenient. Indeed, the double-soft limit followed by the collinear limit of the two soft partons, although obtainable with the formulae of Appendix B, requires a careful evaluation, because of the presence of an apparent quadratic divergence $\sim 1/(q_1 \cdot q_2)^2$ in Eq. (B.8). Of course, the actual leading divergence is only logarithmic as can be checked using colour conservation. To avoid unnecessary complications, we propose to use an iterated limit in which the partons become collinear first, and then produce a soft gluon, which interacts via the usual eikonal current. This is justified by colour coherence of soft emission in the collinear limit, which is usually exploited to derive the soft-collinear limit in which a pair of partons become collinear, and a gluon, not belonging to the pair, becomes soft. The result for our case can be written as follows

$$\begin{aligned} |\mathcal{M}_{c_1 c_2, a_1, \dots, a_n}(q_1, q_2, p_1, \dots, p_n)|^2 &\simeq \frac{2}{s_{12}} g^4 \mu^{4\epsilon} |\mathcal{M}_{a_1, \dots, a_n}(p_1, \dots, p_n)| \\ &\quad \times \mathbf{J}_\mu^\dagger(q_1 + q_2) \hat{P}_{c_1 c_2}^{\mu\nu}(z, k_\perp; \epsilon) \mathbf{J}_\nu(q_1 + q_2) |\mathcal{M}_{a_1, \dots, a_n}(p_1, \dots, p_n)|, \end{aligned} \quad (\text{C.1})$$

where $c_1 c_2 = q\bar{q}$ or gg , $s_{12} = (q_1 + q_2)^2$, \mathbf{J}_μ is the eikonal current defined in Eq. (B.4), and $\hat{P}_{c_1 c_2}^{\mu\nu}(z, k_\perp; \epsilon)$ is the d -dimensional polarized Altarelli-Parisi splitting function given in Eqs. (A.6, A.7, A.8, A.9).

The factorization formula demonstrates the usual spin correlations, which are transferred here to the eikonal currents and not directly to the matrix element, since the nearly on-shell gluon is fully described by the current in the soft limit. One might wonder why the spin correlations survive the soft limit, since they do not at the next-to-leading order. The reason is that the

double-soft limit cannot be defined with the momenta of the collinear pair alone, because the splitting functions depend only on the ratio of the energies of the two partons. Therefore, as long as this ratio remains constant, from the point of view of the collinear limit, we are considering two *hard* partons.

Appendix D. Born level cross sections for top quark pair production

Although text book material, we reproduce these cross sections here for convenience of the reader. We have

$$\sigma_{q\bar{q}\rightarrow t\bar{t}}^B(s, m^2, \alpha_s) = \frac{\alpha_s^2}{m^2} f_{q\bar{q}\rightarrow t\bar{t}}^{(0)}(\beta), \quad \sigma_{gg\rightarrow t\bar{t}}^B(s, m^2, \alpha_s) = \frac{\alpha_s^2}{m^2} f_{gg\rightarrow t\bar{t}}^{(0)}(\beta), \quad (\text{D.1})$$

with

$$f_{q\bar{q}\rightarrow t\bar{t}}^{(0)}(\beta) = \frac{\pi}{6} \frac{T_F C_F}{N} \beta \rho (2 + \rho), \quad (\text{D.2})$$

$$\begin{aligned} f_{gg\rightarrow t\bar{t}}^{(0)}(\beta) &= \frac{\pi}{12} \frac{T_F}{N^2 - 1} \beta \rho \left\{ 3C_F \left[(4 + 4\rho - 2\rho^2) \frac{1}{\beta} \ln \frac{1 + \beta}{1 - \beta} - 4 - 4\rho \right] \right. \\ &\quad \left. + C_A \left[3\rho^2 \frac{1}{\beta} \ln \frac{1 + \beta}{1 - \beta} - 4 - 5\rho \right] \right\}, \quad (\text{D.3}) \end{aligned}$$

and $\rho = 1 - \beta^2$.

Appendix E. Software

The results obtained for the present publication have required the use of numerous software systems. We list them here

- DIAGEN/IDSOLVER, our own private system for diagram generation, analysis and evaluation, has been used for the generation of the cut diagrams and reduction of the integrals needed to compute the volume of the phase space;
- FERMAT [68], an algebra system, is the rational function algebra library of DIAGEN/IDSOLVER, and has been used in the reduction of the phase space integrals;
- FORM [69], has been used for the algebraic simplification of the diagrams, mostly Dirac algebra and color factor evaluation, for which the package COLOR.H has proven useful;
- FORMCALC [70], the backbone of FEYNARTS [71], has been used for the low level formatting of FORTRAN code generated by MATHEMATICA;
- HELAC/PHEGAS [61, 62, 72], has been used for tests of the matrix elements at specified phase space points and checks of the numerical integration routines;
- MATHEMATICA, has been used for the derivation of the subtraction and integrated subtraction terms, convergence tests with very high numerical precision, and generation of FORTRAN code;
- INTEL FORTRAN COMPILER, although not essential for this project, we have used its quadruple precision functionality to spare some minor effort in implementing interfaces to external libraries (see comments in Section 4);
- PARNI [64] adaptive Monte Carlo random number generation optimizer, has been used in the numerical integration routines;
- RANLUX [73, 74], the classic random number generator.

References

- [1] M. Czakon, Phys. Lett. B **693** (2010) 259;
- [2] S. Catani and M. H. Seymour, Nucl. Phys. B **485** (1997) 291 [Erratum-ibid. B **510** (1998) 503];
- [3] S. Catani, S. Dittmaier, M. H. Seymour and Z. Trocsanyi, Nucl. Phys. B **627** (2002) 189;
- [4] S. Frixione, Z. Kunszt and A. Signer, Nucl. Phys. B **467** (1996) 399;
- [5] R. Frederix, S. Frixione, F. Maltoni and T. Stelzer, JHEP **0910** (2009) 003;
- [6] Z. Nagy and Z. Trocsanyi, Nucl. Phys. B **486** (1997) 189;
- [7] T. Binoth and G. Heinrich, Nucl. Phys. B **585** (2000) 741;
- [8] C. Anastasiou, K. Melnikov and F. Petriello, Phys. Rev. D **69** (2004) 076010;
- [9] T. Binoth and G. Heinrich, Nucl. Phys. B **693** (2004) 134;
- [10] A. Gehrmann-De Ridder, T. Gehrmann and E. W. N. Glover, JHEP **0509** (2005) 056;
- [11] A. Daleo, A. Gehrmann-De Ridder, T. Gehrmann and G. Luisoni, JHEP **1001** (2010) 118;
- [12] E. W. Nigel Glover and J. Pires, JHEP **1006** (2010) 096;
- [13] R. Boughezal, A. D. Ridder and M. Ritzmann, arXiv:1011.6631 [hep-ph];
- [14] S. Catani and M. Grazzini, Phys. Rev. Lett. **98** (2007) 222002;
- [15] C. Anastasiou, F. Herzog and A. Lazopoulos, arXiv:1011.4867 [hep-ph];
- [16] G. Somogyi, Z. Trocsanyi and V. Del Duca, JHEP **0506** (2005) 024;
- [17] G. Somogyi and Z. Trocsanyi, arXiv:hep-ph/0609041;
- [18] G. Somogyi and Z. Trocsanyi, JHEP **0701** (2007) 052;
- [19] G. Somogyi, Z. Trocsanyi and V. Del Duca, JHEP **0701** (2007) 070;
- [20] P. Bolzoni, G. Somogyi and Z. Trocsanyi, arXiv:1011.1909 [hep-ph];
- [21] S. Weinzierl, JHEP **0303** (2003) 062;
- [22] W. B. Kilgore, Phys. Rev. D **70** (2004) 031501;
- [23] S. Frixione and M. Grazzini, JHEP **0506** (2005) 010;
- [24] A. Denner, S. Dittmaier, S. Kallweit and S. Pozzorini, arXiv:1012.3975 [hep-ph];
- [25] G. Bevilacqua, M. Czakon, A. van Hameren, C. G. Papadopoulos and M. Worek, arXiv:1012.4230 [hep-ph];
- [26] W. Bernreuther, A. Brandenburg, Z. G. Si and P. Uwer, Nucl. Phys. B **690** (2004) 81;
- [27] K. Melnikov and M. Schulze, JHEP **0908** (2009) 049;
- [28] M. Beneke, M. Czakon, P. Falgari, A. Mitov and C. Schwinn, Phys. Lett. B **690** (2010) 483;
- [29] V. Ahrens, A. Ferroglia, M. Neubert, B. D. Pecjak and L. L. Yang, Phys. Lett. B **687** (2010) 331;
- [30] M. Beneke, P. Falgari and C. Schwinn, Nucl. Phys. B **828** (2010) 69;

- [31] M. Czakon, A. Mitov and G. F. Sterman, *Phys. Rev. D* **80** (2009) 074017;
- [32] S. Moch and P. Uwer, *Phys. Rev. D* **78** (2008) 034003;
- [33] V. Ahrens, A. Ferroglia, M. Neubert, B. D. Pecjak and L. L. Yang, *JHEP* **1009** (2010) 097;
- [34] N. Kidonakis, arXiv:1009.4935 [hep-ph];
- [35] M. Beneke, P. Falgari and C. Schwinn, *Nucl. Phys. B* **842** (2011) 414;
- [36] M. Czakon, A. Mitov and S. Moch, *Phys. Lett. B* **651** (2007) 147;
- [37] M. Czakon, A. Mitov and S. Moch, *Nucl. Phys. B* **798** (2008) 210;
- [38] R. Bonciani, A. Ferroglia, T. Gehrmann and C. Studerus, *JHEP* **0908** (2009) 067;
- [39] R. Bonciani, A. Ferroglia, T. Gehrmann, A. von Manteuffel and C. Studerus, arXiv:1011.6661 [hep-ph];
- [40] R. Bonciani, A. Ferroglia, T. Gehrmann, D. Maitre and C. Studerus, *JHEP* **0807** (2008) 129;
- [41] M. Czakon, *Phys. Lett. B* **664** (2008) 307;
- [42] J. G. Korner, Z. Merebashvili and M. Rogal, *Phys. Rev. D* **77** (2008) 094011;
- [43] B. Kniehl, Z. Merebashvili, J. G. Korner and M. Rogal, *Phys. Rev. D* **78** (2008) 094013;
- [44] S. Dittmaier, P. Uwer and S. Weinzierl, *Phys. Rev. Lett.* **98** (2007) 262002;
- [45] G. Bevilacqua, M. Czakon, C. G. Papadopoulos and M. Worek, *Phys. Rev. Lett.* **104** (2010) 162002;
- [46] K. Melnikov and M. Schulze, *Nucl. Phys. B* **840** (2010) 129;
- [47] Z. Bern, L. J. Dixon, D. C. Dunbar and D. A. Kosower, *Nucl. Phys. B* **425** (1994) 217;
- [48] Z. Bern, V. Del Duca and C. R. Schmidt, *Phys. Lett. B* **445** (1998) 168;
- [49] D. A. Kosower and P. Uwer, *Nucl. Phys. B* **563** (1999) 477;
- [50] Z. Bern, V. Del Duca, W. B. Kilgore and C. R. Schmidt, *Phys. Rev. D* **60** (1999) 116001;
- [51] S. Catani and M. Grazzini, *Nucl. Phys. B* **591** (2000) 435;
- [52] M. Czakon and A. Mitov, *Nucl. Phys. B* **824** (2010) 111;
- [53] A. Gehrmann-De Ridder, T. Gehrmann and G. Heinrich, *Nucl. Phys. B* **682** (2004) 265;
- [54] A. V. Kotikov, *Phys. Lett. B* **254** (1991) 158;
- [55] E. Remiddi, *Nuovo Cim. A* **110** (1997) 1435;
- [56] E. Remiddi and J. A. M. Vermaseren, *Int. J. Mod. Phys. A* **15** (2000) 725;
- [57] S. Catani and M. Grazzini, *Nucl. Phys. B* **570** (2000) 287;
- [58] A. Ferroglia, M. Neubert, B. D. Pecjak and L. L. Yang, *JHEP* **0911** (2009) 062;
- [59] S. Catani, S. Dittmaier and Z. Trocsanyi, *Phys. Lett. B* **500** (2001) 149;
- [60] R. K. Ellis and J. C. Sexton, *Nucl. Phys. B* **269** (1986) 445;
- [61] A. Kanaki and C. G. Papadopoulos, *Comput. Phys. Commun.* **132** (2000) 306;
- [62] A. Cafarella, C. G. Papadopoulos and M. Worek, *Comput. Phys. Commun.* **180** (2009) 1941;

- [63] M. Czakon, C. G. Papadopoulos and M. Worek, JHEP **0908** (2009) 085;
- [64] A. van Hameren, Acta Phys. Polon. B **40**, 259 (2009);
- [65] P. Nason, S. Dawson and R. K. Ellis, Nucl. Phys. B **303**, 607 (1988);
- [66] J. M. Campbell and E. W. N. Glover, Nucl. Phys. B **527** (1998) 264;
- [67] S. Catani and M. Grazzini, Phys. Lett. B **446** (1999) 143;
- [68] R. H. Lewis, Fermat, <http://www.bway.net/~lewis/>;
- [69] J. A. M. Vermaseren, arXiv:math-ph/0010025;
- [70] T. Hahn and M. Perez-Victoria, Comput. Phys. Commun. **118** (1999) 153;
- [71] T. Hahn, Comput. Phys. Commun. **140** (2001) 418;
- [72] C. G. Papadopoulos, Comput. Phys. Commun. **137** (2001) 247;
- [73] M. Luscher, Comput. Phys. Commun. **79** (1994) 100;
- [74] F. James, Comput. Phys. Commun. **79** (1994) 111 [Erratum-ibid. **97** (1996) 357].